CHARACTERIZATION OF MEMBRANE PROTEINS AND LIGAND INTERACTIONS BY NATIVE ION MOBILITY MASS SPECTROMETRY

A Dissertation

by

YANG LIU

Submitted to the Office of Graduate and Professional Studies of
Texas A&M University
in partial fulfillment of the requirements for the degree of

DOCTOR OF PHILOSOPHY

Chair of Committee,	Magnus Höök
Co-Chair of Committee,	Arthur Laganowsky
Committee Members,	David Reiner
	David Russell
	Yubin Zhou
Head of Department,	Warren Zimmer

MAY 2019

Major Subject: Medical Sciences

ABSTRACT

Membrane proteins interact intimately with the lipid bilayer in which they are embedded. Interactions between membrane proteins and ligands such as lipids and other small molecules can affect protein structure and function. Ion mobility-mass spectrometry (IM-MS) has recently emerged as a valuable tool for interrogating the interactions between protein and individual ligands, offering direct measurements such as stoichiometry, molar intensities and gas-phase mobility for each ligand-bound state of a protein complex. This technique is applied to examine the effect of direct ligand binding on model membrane proteins, such as the ammonium channel (AmtB) from *e.coli* and mammalian inwardly rectifying potassium channels (Kir) expressed in *Pichia* yeast. Studies presented here focus on the isolation of direct protein-ligand interactions from ensemble measurements using the model AmtB-lipid complexes, methodologies on mammalian protein preparation for high-resolution native mass spectometry, and the discovery of selectivity of a Kir channel towards the toxin peptide Tertiapin Q (TPNQ) and phosphorylated phosphotidylinositdes (PIPS), an essential signaling lipid required for Kir channel function. Stabilization parameters calculated from isolated AmtB-lipid complexes were compared to ensemble mass measurements to provide insight on the interactions between AmtB and phospholipids, and also provides a basis for methods used for the more complex Kir channels. After optimizing expression and purification methods for the mammalian Kir3.2 (GIRK2) channels for native mass spectrometry, the first high-resolution measurements for GIRK2-lipid complexes and TPNQ binding effects were analyzed. New data revealed that the closed and open states of the channel, as mimicked by a mutant R201A, can tune GIRK2's PIP selectivity such that the open form prefers the PIP isoforms known to activate the channel.

ACKNOWLEDGEMENTS

I would like to thank my advisor, Dr. Laganowsky, and all my committee members, Dr. Magnus Höök, Dr. David Reiner, Dr. David Russell and Yubin Zhou for their guidance and support throughout the course of this research. Dr. Wen Liu, a former co-worker of our group and close colleague, also acted as a mentor during my graduate studies. Special thanks to Cynthia Lewis for her support and assistance on administrative matters.

Thanks also to my friends, colleagues, the department faculty and staff for making my time at Texas A&M University a great experience.

CONTRIBUTORS AND FUNDING SOURCES

Contributors

This work was supervised by a thesis (or) dissertation committee consisting of Professor Arthur Laganowsky (advisor) and David Russell of the Department of Chemistry, Professors Magnus Höök, David Reiner and Yubin Zhou of the TAMHSC Institute of Biosciences and Technology.

Cloning work in Chapter I and Chapter II was conducted by Dr. Wen Liu of the TAMHSC Institute of Biosciences and Technology. All other works conducted in this dissertation was completed by the student independently or with input from the advisor.

Funding Sources

Graduate study was supported by Professor Laganowsky's faculty start-up funds.

This work was also made possible in part by National Institutes of Health (NIH) under Grant Number DP2GM123486.

NOMENCLATURE

MS	Mass Spectrometry
IM	Ion Mobility
AmtB	Ammonium Channel (from *e.coli*)
GIRK2	G-protein Activated Inwardly Rectifying Potassium Channel 3.2 / Kir3.2
CIU	Collision Induced Unfolding
ATD	Arrival Time Distribution
DDM	n-Dodecyl-β-D-Maltopyranoside
C8E4	Tetraethylene glycol monooctyl ether
C10E5	Pentaethylene glycol monodecyl ether
PIP	Phosphorylated Phosphatidylinositides
Top-Down MS	Mass spectral analysis where the protein is intact
Bottom-Up MS	Mass spectral analysis where the protein is digested and then fragmented

TABLE OF CONTENTS

LIST OF FIGURES

LIST OF TABLES

Page

CHAPTER I

INTRODUCTION TO NATIVE ION MOBILITY MASS SPECTROMETRY (IM-MS)

Membrane proteins interact intimately with the lipid bilayer in which they are embedded [1]. Many vital cellular processes rely on membrane proteins and their function, including trafficking and signal transduction [2-4]. Analyses in the past decade show that over half of all drugs on the market target integral membrane proteins [5, 6]. Detailed understanding of how lipids affect the structure and function of proteins is therefore important for understanding fundamental biological processes and diseases. Recently, mass spectrometry (MS) approaches have emerged that can quantify individual binding events of protein-ligand complexes, and when performed in unison with an ion mobility device, ions are separated based on their shape and charge. This method, referred to as Ion mobility mass spectrometry (IM-MS), provides insight into protein conformation by reporting on the rotationally averaged collision cross section [7, 8].

Nano electrospray ionization is routinely employed to introduce intact protein complexes into a mass spectrometer that is tuned to maximize desolvation – the liberation of protein complexes from solvent droplets – and minimize activation of the ions to retain solution-state structures [9, 10]. Depending on the instrument, desolvation, including activation, can be accomplished, for example, through adjusting source pressure, source temperature, and increasing the potential on specific elements, such as “cone” voltage (a number of review articles discuss this in further detail [11-14]). More specifically, increasing source temperature, for example using a heated-capillary, can effectively desolvate ions through “in-source” collisional

activation, however elevated temperatures can lead to dissociation of noncovalent soluble protein complexes [15-20].

Mass spectra of membrane protein complexes recorded under instrument settings typically used for soluble proteins often result in a large, unresolved hump [9, 21, 22]. Thus, membrane proteins require a larger degree of activation, which is typically achieved in the trap or collision cell of the instrument, in order to desolvate, liberate them from the detergent micelles, and yield resolved mass spectra [9, 21, 23-25]. Although membrane proteins require more activation compared to their soluble counterparts, the excess detergent and lipid form a protective layer that protects them during activation such that native-like conformations can be observed by ion mobility post-detergent removal [21, 26-28]. Minimal increases in energy (above the threshold to strip detergent from the membrane protein complex) can perturb membrane protein structure, similarly to soluble proteins [27].

IM-MS is well suited for recording collision-induced unfolding (CIU) profiles of ions by measuring their mobility post collisions with neutral gas molecules in the trap, which can provide useful information for molecular analysis [29, 30] Such methods have been used to describe conformation and stability of large protein complexes and how events such as ligand binding can affect their structure [9, 30-33]. Unlike other biophysical approaches, where typically the observable is the ensemble of species (*apo* protein and ligand-bound states) in solution, IM-MS is capable of resolving individual protein-ligand binding events and characterizing their structural and conformational effects. For example, one study distinguished the class of ligand bound to a protein kinase, a soluble protein, by their CIU profiles [34]. Of

late, CIU-based quantitative IM-MS methods have been developed to determine how lipid-binding events stabilize membrane protein complexes [27, 35]. Using the software program Pulsar [35], we can easily generate CIU profiles for *apo* and lipid bound states and use algorithms to quantify the transitions in the unfolding pathway. The stability afforded by the bound lipid is calculated by the sum of the differences between transitions in the CIU profiles for *apo* and lipid bound states. This IM-MS method used in earlier works demonstrated that different lipids can stabilize membrane proteins to varying degrees, with the most stabilizing lipids modulating the structure and function of membrane proteins [27]. As an example, a previous study have shown that the activity of the bacterial water channel aquaporin Z can be modulated nearly three-fold by the binding of cardiolipin, a lipid that significantly stabilized the channel in IM-MS studies. However, the molecular mechanism behind the increased activity remains unclear. More details on how this technique interrogate protein complexes, especially membrane proteins, will be helpful for studying more challenging systems, such as eukaryotic membrane complexes.

CIU profiles of membrane proteins are typically performed on the entire ensemble (*apo* and lipid bound species) that raises uncertainty to the contribution of individual lipids and the species that are ejected in the unfolding process. During the CIU process, where collision voltage is increased in a stepwise fashion, the bound ligand(s) may eject from the complex as neutral or charged species. If the ligand ejects as a neutral, the signal from remaining charged species will contribute to the signal minus the mass of the ejected ligand, giving rise to heterogeneity of distinct *apo* and ligand bound states. In contrast, a ligand ejected as charged species could alter the initial charge state of the ion, such as for collisionally activated dissociation of ribonucleases

in complex with nucleotides [36], and the signal for charge-stripped ion would contribute to neighboring ion(s). As current CIU methods for membrane proteins do not isolate ions prior to collisional activation, the CIU profile for a given *apo* or lipid bound state can be compromised by overlapping ions that are the product of the protein complex minus lipid(s) ejected as either neutral or charged species. Our studies mainly focuses on the further development of existing IM-MS methods to probe membrane protein lipid interactions. We employed mass spectrometry ion mobility mass spectrometry (MS-IM-MS), which has been shown to allow for greater depth of information [37, 38]. In this dissertation, two membrane protein systems will explored. The first being the ammonia channel (AmtB) from *Escherichia coli* as a model membrane system for establishing the methodology, and the second being a mammalian inwardly rectifying potassium channel for further biophysical details on ligand interaction and selectivity.

CHAPTER II*

NATIVE IM-MS STUDY OF AMTB

We selected the trimeric ammonia channel (AmtB) from *Escherichia coli* as the model integral membrane protein to bind to select phospholipids, some of which details have been described in other studies [9, 27, 39]. In the Synapt G1 instrument [40] the quadrupole is located before the collision cell, where collisional activation is typically applied to membrane proteins [27], making it a necessity to have a resolved mass spectrum prior to entering the quadrupole in order to isolate specific ions. In this study, we investigated higher source temperatures as a source of "in-source" collisional activation to release membrane proteins lipid complexes from the detergent micelle. By this method, we could record resolved mass spectra prior to entrance into the quadrupole and for the first time isolate ions of AmtB-lipid complexes in the quadrupole. After successfully isolating specific lipid-bound states of AmtB, we generated CIU profiles by collisional activation in the collision cell, which is located after the quadrupole. These CIU profiles are free of ensemble effects, such as contributions from product ions that have ejected lipid(s). We then compare results from IM-MS and MS-IM-MS approaches to provide insight into how CIU profiles can be affected by lipid ejection and the relationship to measured biophysical parameters.

*Reprinted with permission from "Characterization of Membrane Protein–Lipid Interactions by Mass Spectrometry Ion Mobility Mass Spectrometry" by Liu *et al.*, 2016, J Am Soc Mass Spect. 28, 579-586, Copyright 2016 by Spring Nature

Methods in Studying the Prokaryotic Channel AmtB

Protein expression and purification

The ammonia channel (AmtB) was expressed and purified from *Escherichia coli*. AmtB (residues 26-428) gene was amplified by polymerase chain reaction (PCR) with Q5 high-fidelity DNA polymerase (New England Biolabs). pET15b vector (Novagen) was linearized by XhoI (New England Biolabs) and gel purified (QIAquick Gel Extraction Kit, Qiagen), and used in an In-Fusion cloning reactions (Clonetech) to generate a TEV protease cleavable C-terminal fusion to maltose binding protein preceded by a secretion signal peptide (pelB) and 6x His-tag sub-cloned from Hilf *et al.*[41]. The resulting vector was linearized with NdeI and NheI (New England Biolabs), gel purified and used in subsequent In-Fusion cloning reactions along with AmtB PCR products and primers designed for an In-Fusion cloning reaction to generate AmtB-MBP expression plasmids. The plasmid was transformed into E. coli BL21 (DE3) ArcticExpress (Agilent) competent cells. Colonies grown on selection plates were inoculated into 50 mL Luria Broth (LB) and grown overnight at 37 °C, One liter Terrific Broth (TB) in 2 liter shaker flasks were inoculated with 4 ml of overnight culture and grown at 30 °C until the culture reached OD_{600nm} between 0.6 to 0.8. Flasks with culture were chilled in an ice water bath for 10 minutes for cold-shock, and Isopropyl β-D-1-thiogalactopyranoside (IPTG) was added to the culture at a final concentration of 0.5 mM. The culture is then grown overnight at 30 °C before cells were collected. Cell pellets were formed by centrifugation at 5,000g for 10 min at 4 °C, and then resuspended in Tris-buffered saline (TBS), pelleted by centrifugation at 5,000g for 10 min at 4 °C and stored at −80 °C. Cell pellets were thawed and resuspended at 20 mL per litre of culture in buffer A (300 mM sodium chloride, and 20 mM 2-amino-2-hydroxymethyl-propane-1,3-diol

(Tris), pH 7.4 at room temperature) supplemented with a complete protease inhibitor tablet (Roche). The cell suspension was passed 3 times through an M-110 microfluidizer (Microfluidics) at 20,000 psi. Insoluble material was pelleted by centrifugation at 20,000g for 25 minutes at 4 °C. The supernatant from the lysate was centrifuged again at 115,000g for 2 hours at 4 °C to pellet the membranes. Membrane pellets were resuspended in ice-cold buffer B (150 mM sodium chloride, 20% glycerol, 5 mM BME and 20 mM Tris, pH 7.4 at room temperature), homogenized using a Dounce tissue grinder (Wheaton Glass). AmtB-MBP was extracted from homogenized membranes in buffer B supplemented with 2.5% DDM (n-Dodecyl-β-D-Maltopyranoside, Anatrace) overnight at 4 °C on a rotating mixer set to gentle speeds. Extracted membrane proteins were clarified by centrifugation at 40,000g for 25 min at 4 °C, and the supernatant was filtered before loading onto a 5 mL HisTrap-HP column (GE Healthcare) equilibrated in buffer C (150 mM sodium chloride, 10% glycerol, 20 mM imidazole, 0.025% DDM and 50 mM Tris, pH 7.4 at room temperature). After the clarified supernatant was loaded, the column was initially washed with 20-30 mL of buffer C supplemented with an additional 0.5% of DDM, and the membrane proteins were exchanged into buffer E until a steady baseline for UV absorbance at 280 nm was achieved. AmtB-MBP were eluted with a linear gradient from 10% to 100% buffer D (100 mM sodium chloride, 10% glycerol, 500 mM imidazole, 0.025% DDM and 50 mM Tris, pH 7.4 at room temperature) over 15 mL, and peak fractions were pooled. The fusion protein solution was loaded through a 26/10 desalting column desalting (GE Healthcare) equilibrated in buffer C to remove excess imidazole, and peak fractions were once again pooled. The fusion protein is then supplemented with 5mM bME (β-mercaptoethanol) and his-tagged TEV protease and allowed to incubate overnight at 4 °C. The solution was then filtered and passed through a 5mL HisTrap-HP column again equilibrated in buffer C, with flow-

through containing the untagged AmtB protein which is collected and concentrated using a 100kDa molecular weight cut off filter. Notably, the AmtB protein with its C-terminal tags removed contained the additional protein sequence ASGENLYFQ, resulting from the TEV protease recognition sequence and cloning restriction site. Concentrated protein was either used immediately or flash-frozen in liquid nitrogen and stored at -80 °C.

Sample preparation for native mass spectrometry

Flash-frozen AmtB samples thawed on ice or freshly prepared samples were detergent exchanged by size exclusion chromatography (SEC). Membrane protein samples were injected onto a superdex 200 GL 10/200 SEC column (GE Healthcare) equilibrated in buffer E (150 mM sodium chloride, 10% glycerol and 50 mM Tris, 0.5% tetraethylene glycol monooctyl ether, pH 7.4 at room temperature). Peak fractions containing the detergent-exchanged AmtB protein were collected and concentrated using a 50 kDa molecular weight cut off filter, and is either used directly or flash-frozen in liquid nitrogen and stored at -80 °C. It is important to note that C8E4, or tetraethylene glycol monooctyl ether, act as a cryoprotectant along with the glycerol in buffer E, and there are no observable differences in mass spectra quality after freeze-thaw of a well-purified AmtB sample. The protein is buffer exchanged into mass spectrometry buffer AA, or 200 mM ammonium acetate containing 0.05% C8E4, pH 7.5 (by ammonium hydroxide) using a centrifugal buffer exchange device (Micro Bio-Spin 6 columns, Bio-Rad).

Stock solutions of synthetic phospholipids with 16:0-18:1 acyl chains (Avanti Polar Lipids Inc., Alabama, USA) were purchased dissolved in chloroform. Hamilton syringes were used to aliquot the appropriate amount of chloroform solution into a glass vial, and a lipid film

was made by applying a constant stream of nitrogen gas. The lipid aliquot was further dried inside a desiccation chamber overnight, and then dissolved in AA buffer supplemented with 0.5% C8E4 and 5 mM 2-mercaptoethanol (β-ME). 4 uL of AmtB protein solution (at 80 nM) was mixed with 4 uL of lipid solution (at 8 uM) to form a AmtB-lipid complex, incubated at room temperature for 2 minutes, and the mixture is back filled into a gold-coated glass emitter. The glass emitters were made by pulling glass capillaries (Sutter Instrument) using a Sutter P-97 micropipeete puller, and gold-coated with a Leica EM ACE600 sputter coater.

Protein and Lipid Quantification

Protein concentration was determined with the DC Protein Assay kit (Bio-Rad) using bovine serum albumin as the standard. Phospholipid concentration was determined by phosphorous analysis [42, 43].

Ion Mobility-Mass Spectrometry (IM-MS)

IM-MS and MS-IM-MS were performed on a Synapt G1 HDMS instrument (Waters Corporation) equipped with a radio frequency generator to isolate higher *m/z* species (up to 32k) in the quadrupole, and a temperature-controlled chamber attached to the source region and sample inlet in order to minimize changes in solution temperature due to changing instrument settings in the source region as well as atmospheric disturbances. Instrument parameters were tuned to maximize signal intensity for IM-MS and MS-IM-MS while preserving the native-like state of AmtB. The source temperature was set to 23 (ambient), 40, 80, or 120 ºC, capillary voltage of 1.7kV, sampling cone voltage of 200V, extractor cone voltage of 10V, argon flow rate in the trap was set to 7 mL/min (5.2×10^{-2} mbar), and transfer collision energy at 15V. The T-

wave settings were for trap (300 ms^{-1}/1.0V), IMS (300 ms^{-1}/20V) and transfer (100 ms^{-1}/10V), and trap DC bias (35V). CIU was performed from 10V to 200V on trap collision energy in 10V steps. For MS-IM-MS, the quadrupole LM resolution was set to 6. To minimize differences caused by variations in gold-coated glass capillary tips, each replicate was collected from one tip using the same preparation of protein-lipid mixture.

Data Processing and Analysis

IM-MS and MS-IM-MS data were processed with the software program Pulsar [35]. The intensities of protein and protein-lipid species were deconvoluted and converted to mole fraction using UniDec [44].

Results and Discussion

Activation of membrane protein complexes for MS-IM-MS

As a step towards MS-IM-MS of membrane protein complexes, we set out to develop methods to activate membrane proteins in the source region such that resolved ions can confidently be isolated in the quadrupole prior to entering the collision cell. Starting with a modest trap collision voltage setting of 20V and a maximum setting for the cone voltage (200V), the mass spectrum we obtained at ambient source temperature (23 °C) was poorly resolved and not ideal for isolating *apo* and lipid bound states of AmtB (Fig 1). To further activate ions upstream in the instrument, we then explored raising the source temperature from ambient to 40, 80, and 120 °C. With increasing source temperatures we observed an overall increase in signals for resolved AmtB species, especially for the lower charge states of the protein complex (Fig 1). It is unclear why there is an increase in abundance of lower charge states at elevated source temperatures, but plausible explanations could be charge stripping in the source region, or improved desolvation for lower charge state ions in the instrument. Interestingly, increasing source temperature under modest trap settings resulted in resolved mass spectra comparable to that collected at ambient source temperature with 60V applied to the collision cell. Thus, elevated source temperature can provide sufficient "in-source" collisional activation to liberate AmtB from the detergent micelle.

CIU profiles acquired by IM-MS and MS-IM-MS

We then carried out a series of experiments at different source temperatures to understand the impact of elevated source temperature on CIU of AmtB bound to lipids (Fig 2). Herein we

focus on the 15^+ charge state of AmtB bound to lipid(s) since their CIU profiles have been previously characterized and peer-reviewed [27]. The first transition from a native-like state, where the measured collision cross section (CCS) agrees with the calculated CCS for AmtB [27], decreases roughly by 20V with each 40 °C increase in source temperature (Fig 2a). A similar drop in collision voltage for the two subsequent transitions was observed as well. We speculate that the change in the collision voltage required to unfold the AmtB-lipid complexes to be the result of an overall increase in internal energy. This would be consistent with reports for soluble system, where increased "in-source" activation raises the internal energy of ions and lowers the collisional activation post-source to fragment or dissociate noncovalent complexes [17, 45]. Moreover, we also observed an increase in the width of the arrival time distribution (ATD) for all species with increasing source temperature and the native-like ATD nearly doubling in width. The cause behind this interesting observation is unclear, but one plausible explanation is that there are contributions from other ions that have either ejected bound lipids or charge-stripped in the collision cell.

Given our ability to isolate ions of AmtB-lipid complexes, we recorded CIU profiles of AmtB bound to two lipids by collisional activation in the collision cell, which is located after the quadrupole (Fig 2b). After isolating the ions corresponding to the 15^+ charge state of AmtB bound to two 1-palmitoyl-2-oleoyl (PO) phosphatidic acid (POPA) lipids, we subjected these ions to increasing trap collision voltage to record MS-IM-MS CIU profiles. In contrast to IM-MS CIU profiles, the unfolding transitions occurred at significantly lower trap collision voltage. For example, at a source temperature of 40 °C the first transition was at 75V versus 130V for IM-MS and MS-IM-MS, respectively. In addition, the drop in transition collision voltage with increasing

source temperature was roughly 7V, approximately a third of the value observed in IM-MS. Last but not least, the width of the ATD was consistent among the source temperatures tested, implying that source temperature is not responsible for ATD widening observed in IM-MS. Most interestingly, we noted a faint transition occurring around ~75V that coincidentally matched the first transition observed in the MS-IM-MS CIU profile (Fig 2a-b, left panels). Upon closer examination, it appears there is an *apo* MS-IM-MS CIU profile that faintly underlies the profile acquired by IM-MS, specifically weak ATD distributions starting to appear at 8 and 10 milliseconds and from collision voltages indicated by arrows. Taken together, our results provide evidence that IM-MS CIU profiles of protein-lipid complexes can be heterogeneous, which we hypothesize is due to the contribution from product ions after ejection of their bound lipid(s).

Ejection of bound lipid(s) from AmtB during CIU

To understand how bound lipids eject from AmtB, we first examined the mass spectra in IM-MS CIU profiles. In general, we observed a gradual decrease in signals corresponding to AmtB bound to lipid with increased collision voltage (Fig 3a). We then investigated mass spectra in MS-IM-MS CIU profiles. The signal for the isolated 15^+ charge state of AmtB bound to two lipids was absent at a trap collision voltage above 160V (Fig 3b), which is dramatically different from IM-MS profiles where lipids remained present even above collision voltage settings of 200V (Fig 3a, Fig 5). After examining mass spectra for MS-IM-MS profiles of AmtB bound to two PO phosphatidylglycerol (POPG) molecules, we observed that even though AmtB$(POPG)_2$ gradually lost both bound lipids with increased trap collision voltage, the charge state of AmtB remained the same (Figure 3b), indicating that the bound lipids ejected as neutral (without charge) species. Interestingly, we could obtain a CIU profile for the product of AmtB$(POPG)_2$

minus one POPG, yielding AmtB(POPG)$_1$ (Fig 4a). Analysis of MS-IM-MS CIU profiles for AmtB bound to other lipids gave similar results, even when selecting ions corresponding to AmtB bound to one lipid (Fig 4b). Notably, all lipids investigated in this study ejected from AmtB as neutral species. Thus, the product ions after ejection of their bound lipid(s) in the CIU process compromise other ions of the same charge state but lower in mass *i.e.* mass minus the ejected lipid(s).

To gain further insight into the lipid ejection process during CIU, we plotted the mole fraction of AmtB species from IM-MS and MS-IM-MS CIU profiles (Fig 5). As seen by IM-MS CIU profiles, the PO-type lipids have similar trends but slightly differ in the initial transition point where lipids start to eject. In contrast, the mole fraction of bound tetra oleoyl (18:1) cardiolipin (TOCDL) is fairly constant, with a ~14% change in the fraction of *apo* AmtB across the CIU profile. We then plotted the mole fraction for AmtB species derived from MS-IM-MS CIU profiles for AmtB bound to one (1x) or two (2x) lipids (Fig 5b-c). Similar to IM-MS, all the PO-type lipids exhibited similar patterns. However, an initial lipid loss occurring early on in the CIU profile doesn't appear in the mole fraction plot from IM-MS. TOCDL was virtually constant with some ejection at higher collision voltage settings and an absence of *apo* AmtB for MS-IM-MS 2x. The discrepancy for TOCDL dissociation is intriguing, but similar observations have been observed for some soluble protein-ligand systems [12, 36]. In general, the rapid ejection of lipid in general appears to happen at collision voltages where the third and fourth partially unfolded intermediates begin to appear in the CIU profile. It is also worth noting that these mole fraction plots can be a useful reference for quantifying lipid binding on other instruments, such as the Orbitrap [46].

IM-MS and MS-IM-MS derived stabilization of AmtB lipid binding

After establishing that lipids are ejected from AmtB as neutral species, we set out to determine the stabilization afforded by AmtB binding one and two lipids using IM-MS and MS-IM-MS CIU profiles (Fig 6). The calculated stabilization for AmtB binding one lipid determined from IM-MS and MS-IM-MS CIU profiles are similar with IM-MS giving slightly higher values. The stabilization values for 1x are statistically indistinguishable, which is in agreement with our recent report on the thermodynamics of these lipids binding AmtB [39]. There is slight deviation for the binding of two lipids, where stabilization for binding of two lipids is the greatest for IM-MS CIU profiles. The products of lipid ejection contributing to CIU profiles can in part explain the increase in stability. More specifically, this effect could potentially be enhanced for some lipids that readily dissociate from AmtB, providing a rationale for the increase in stabilization for the second lipid-binding event in some cases. In support of this idea, POPG and POPE have the most pronounced increase in AmtB stabilization for the second lipid-binding event, and these lipids appear to dissociate more readily from AmtB (see Fig 5c). Furthermore, stabilization for AmtB binding TOCDL, a lipid that does not readily eject from the complex, is indistinguishable. In short, the effects of lipid ejection on CIU profiles are enhanced for lipids that readily dissociate, and IM-MS and MS-IM-MS yield similar ranking of lipids that stabilize AmtB.

As we used the same lipids in our recent study [39], we set out to compare stabilization values to equilibrium dissociation constants (K_D). We found no correlation between the stabilization values and K_D. The discrepancy between these two values could be rationalized by the unfolded protein and unfolded protein-lipid (or protein-ligand) complex differing in energy landscape, making the stabilization energy not equal to the binding energy of a ligand [39].

Summary and Conclusions

Lipids have essential roles in the folding, structure, and function of membrane proteins [1-3, 27, 47-49], and the development of new methods to elucidate how lipids exert their effects are of great biological importance. Here, we describe the application of "in-source" collisional activation of membrane protein complexes to produce resolved ions that can be isolated in the quadrupole of a Waters Synapt G1 instrument while preserving their native-like structure in the gas-phase. Using this method, we collected for the first time MS-IM-MS CIU profiles for a membrane protein in complex with lipid. This led to the finding that bound lipids eject from AmtB as neutrals, which gives rise to overlapping CIU profiles when using the IM-MS CIU method. This study have also shown that the stability for AmtB bound to different lipids do not vary significantly between IM-MS and MS-IM-MS measurements, and no correlation to biophysical parameters, such as K_D, was found. This method to desolvate and isolate ions of membrane protein complexes will be advantageous for other MS methods, such as ultraviolet photodissociation [50] and surface induced dissociation [51, 52]. Most importantly, the robust technique and detailed understanding on the interpretation of IM-MS data will set the foundation on which more challenging protein systems can be studied. In the following chapter, a more complex mammalian potassium channel will be also subjected to a similar IM-MS method under native-like conditions.

CHAPTER III

CHARACTERIATION OF MOUSE GIRK2 CHANNELS AND INTERACTIONS WITH SIGNALING LIPIDS AND TOXIN

Introduction to GIRK2 Channels

With the establishment of robust native ion mobility mass spectrometry methods for quantitative measurements on membrane proteins, a more complex channel with well-established interactions with specific signaling lipids becomes an interesting candidate to interrogate. Inward rectifying potassium (IRK) channels are a family of membrane protein complexes that transport potassium ions across biological membranes into cells whereas outward flux is blocked by intracellular polyamines and magnesium [53, 54]. These channels are involved in numerous physiological processes, such as neuronal signaling, heart rate regulation and potassium homeostasis [54-56]. Mutations in IRK channels underlie a number of diseases including Andersen syndrome, Bartter syndrome and neonatal diabetes [57-59]. Activation of IRK and a number of other channels requires the signaling lipid phosphatidylinositol 4,5-bisphosphate ($PI(4,5)P_2$), which represents a minor component of the cytoplasmic leaflet [60-68]. IRK channels are also regulated by a number of other molecules including anionic lipids, sodium, ethanol, and toxins [54, 69-76].

Atomic structures have revealed detailed interactions of $PI(4,5)P_2$ with dioctanoyl (8:0-8:0) acyl chains binding to chicken IRK2 (Kir2.2) and mouse G-protein gated IRK2 (GIRK2, Kir3.2) [64, 77, 78]. These structures reveal a similar fold with one $PI(4,5)P_2$ bound per subunit

at the interface between the transmembrane domain (TMD) and cytoplasmic domain (CTD). The negatively charged, phosphate-rich head group of $PI(4,5)P_2$ promotes coordination with lysine residues and backbone amides on GIRK2 [77]. $PI(4,5)P_2$ binding to GIRK2 induces a slight rotation of the inner helix but insufficient to open the channel. An open, gated conformation is only achieved as a result of a four degree rotation of the CTD upon $G_{\beta\gamma}$ binding between adjacent CTD subunits. The R201A mutation of GIRK2 ($GIRK2^{R201A}$) does not require $G_{\beta\gamma}$ binding to gate and the structure in complex with $PI(4,5)P_2$ is in a gated conformation; However, there is an exaggerated rotation of the CTD compared to the gated wild-type channel. $GIRK2^{R201A}$ has been proposed to be a mimic of the $G_{\beta\gamma}$-protein activated state [77] and provides an opportunity to study the effect of the CTD orientation on PIP binding.

In addition to $PI(4,5)P_2$, electrophysiology studies have revealed the other six PIP isoforms can gate IRK subfamilies to various degrees [62, 68, 71, 79, 80]. For example, IRK1 (Kir2.1) is activated primarily by $PI(4,5)P_2$ but the channel appears to bind other PIPs with similar affinity [62, 80]. The hetero-tetrameric GIRK1/GIRK4 channel, which is in the same subfamily as GIRK2, can be activated with similar efficacy by $PI(4,5)P_2$, $PI(3,4)P_2$, $PI(3,5)P_2$ and $PI(3,4,5)P_3$ [68]. ATP-sensitive potassium channels (K_{ATP}) are IRKs that are promiscuously activated by PIPs [62]. Moreover, GIRK1/GIRK4 has a strong dependence on the acyl chain chemistry of the PIP with the greatest activation for 18:0-20:4 tails [68], which is the most abundant form in mammalian cells [81]. In contrast, IRK1 does not display a preference towards the acyl chains of PIPs [68, 80]. Although functional assays report an overall pharmacological shift and not on the stoichiometry of bound PIPs, these studies demonstrate that IRKs are distinctly activated by PIP isoforms. In addition, anionic lipids, such as phosphatidylglycerol, not

only are required for gating of Kir2 channels but also increases sensitivity of Kir2 toward PIPs by ten to one-hundred fold [71, 82]. With these findings in mind, there is an emerging necessity for novel approaches to interrogate individual PIP binding events to these tetrameric ion channels in order to gain chemical insight into the impact of PIP isoforms and acyl chain chemistry on binding.

Native mass spectrometry (MS) is a powerful biophysical technique for investigating membrane proteins and their interactions with small molecules, such as lipids [27, 32, 39, 83]. As mentioned in the previous chapter, native MS can interrogate individual ligand-binding events to protein complexes while preserving non-covalent interactions in the mass spectrometer [27, 84-87]. To expand on the importance of this point and to provide an example, native MS coupled with a temperature controlled source has been used to obtain thermodynamics for membrane protein interactions with lipids and protein [39, 88]. Notably, thermodynamic parameters for protein–ligand and protein-protein interactions determined using other biophysical techniques, such as isothermal titration calorimetry and surface plasmon resonance, are in agreement with those obtained using native MS [39, 88, 89]. Although an improperly tuned instrument could adversely affect the fraction of lipid bound to the protein [87], prior native MS studies [39, 88, 89] establish that a properly tuned instrument can measure equilibrium binding constants and thermodynamic parameters comparable to those measured in the solution phase. Moreover, MS has also revealed that specific protein-lipid interactions can stabilize protein complexes[27, 90] and allosterically modulate other interactions with protein [88], lipids [91], and drugs [83, 92]. This capability will be utilized in fundamental understanding of how channels such as GIRK can interact with its activator lipid, PIPs.

Although native MS has provided insight into a handful of membrane protein complexes, the rate-limiting step to obtaining a high-resolution mass spectrum – a prerequisite for detailed biophysical studies – is often frustrated by sample preparation and quality [9]. These challenges in general are exacerbated for eukaryotic membrane proteins, such as for G-protein coupled receptors, requiring considerable effort to optimize their purification [93]. Here, we optimized the purification of the mammalian GIRK2 channel for high-resolution native MS studies such that small molecules could readily be resolved. We then used native MS to study the binding of small molecules and PIP isoforms including different acyl chains to GIRK2 and the R201A mutant of GIRK2 that displays a rotation of the CTD similar to that when in complex with PIP and $G_{\beta\gamma}$ [77].

Methods and Troubleshooting

Construct preparation and expression of recombinant mouse GIRK2 in Pichia pastoris

For construction of the GIRK2 expression plasmid, the KCNJ6 gene from *Mus musculus* (amino acid 52-380 used for structure determination [77]) was codon optimized for *Pichia pastoris* using the Codon Optimization Tool from Integrated DNA Technologies (IDT) and synthesized as a gBlocks gene fragment (IDT). The pPICZ vector to express chicken Kir2.2 was a generous gift from Dr. Roderick MacKinnon and subsequently modified to have terminal StrepII tag and 6xHis-tag for protein purification and eGFP to enable quantitation of recombinant protein expression. This vector was also modified to contain a TEV (Tobacco Etch Virus) protease site between the protein of interest and the purification/quantitation tags. In-Fusion cloning kit (Clontech) was used to clone the codon optimized GIRK2 gene fragment into the modified pPICZ vector linearized with XhoI and EcoRI (New England BioLabs). This produced a construct which can express GIRK2-eGFP-StrepII-6xHis fusion protein under the control of the inducible alcohol oxidase promoter with eGFP used as a reporter of protein expression. The R201A mutant was generated using the QuikChange Lightning Site-Directed Mutagenesis Kit (Agilent) following manufacturer's protocol. The resulting plasmids were verified by restriction digest analysis and DNA sequencing.

The components of the recombinant protein could be arranged in ways such that either purification tag can be on the N- or C-terminus of the protein, or with both tags on one side in different orders. Several iterations of constructs were screened for both Kir2.2 and GIRK2, and a summary of the different expression efficiency and qualities by the different construct is as

follows. N-terminal StrepII tag causes the absence of protein expression while C-terminal StrepII-tagged recombinant protein can express properly, even though linker peptide and TEV sites separate the tag and the Kir/GIRK sequences. 6xHis tag does not interfere with expression on either N- or C-terminus. The resulting recombinant protein expressed, either from the N-6xHis-Tev-GIRK2-TEV-eGFP-StrepII-C construct, or the N-GIRK2-TEV-eGFP-StrepII-6xHis-C construct, expresses as a stable tetramer. The quality of the expressed recombinant protein from the two constructs seems comparable, but further validation by denatured, or top-down mass spectrometry would be necessary in order to accurately determine the sequence integrity of each monomer. Some work have been done to show that monomers of expressed recombinant kir channels can be phosphorylated multiple times, giving rise to heterogeneity in mass. Regardless, the N-GIRK2-TEV-eGFP-StrepII-6xHis-C was used in this study, and the pPICZ plasmid containing this construct was linearized with PmeI (New England BioLabs) before transformation into *P. pastoris* KM71.

P. Pastoris strain and transformation comparison

Three strains tested for expression of GIRK2 were KM71, GS115 and SuperMan. Among them, KM71 and GS115 had moderate transformation efficiency by either electroporation or chemical transformation, while SuperMan showed markedly lower transformants. In addition, SuperMan transformants are observed as small, slowly dividing cells that tend to clump together when observed under a microscope, compared to the other two strains. The differences in the purified protein from different strains were not significant. The protein used in this study was purified from KM71 strain of transformants. It is necessary to empirically determine the optimal transformation method and growth conditions for generating well-expressing transformants.

Clonal selection and expansion

Transformants were selected on YPD plates containing 0.6 M sorbitol, 500 to 1,000 μg/mL zeocin and 2% agar. All the tested recombinant clones showed a methanol utilization plus or Mut^+ phenotype. The *P. pastoris* integrant colony which showed highest eGFP level (*i.e.* greenest color) during small-scale expression screening (15 mL culture after 30 hours post induction with methanol) was used for large-scale expression. This step was closely monitored for possible bacterial contamination, which prevented adequate expression of protein. To minimize this, all media were supplemented with either kanamycin/ampicillin at 50 and 100 ug/mL respectively, or penicillin/streptomycin mixture at 1:10 working concentration. To produce starter culture, a single colony of *P. pastoris* GS115/pPICZB-GIRK2-eGFP-StrepII-6xHis was grown (27 °C, 220 rpm) for 20 hours in BMGY media (1.34% yeast nitrogen base, 1% yeast extract, 2% peptone, 0.1 M potassium phosphate, pH 6.1, 1% glycerol, 0.4 μg/ml biotin, and 40 μg/mL histidine) containing 150 μg/mL zeocin. Cells were pelleted (1,500 g, 10 min) and then resuspended in BMMY media (BMGY medium without glycerol but with 1% methanol) for induction with methanol. Harvesting cells may introduce unwanted bacterial contamination, so care should be taken here, including autoclaving centrifuge bottles, practicing sterile techniques, etc. Cultures were grown (27 °C, 220 rpm) for roughly 40 hours with addition of 0.5% methanol twice daily, with the first methanol addition to contain 0.1% polypropylene glycol 2000 as an anti-foaming agent (this seems to help maintain consistency in expression and microbe health). Longer expression time produces more protein, but can cause issues such as increased bacterial contamination, or the truncation of all expressed protein. Color, consistency, odor and cell shape must be checked before cells are to be harvested. Mixing contaminated cells or dying cells with healthy expression cells will cause unwanted heterogeneity in downstream

analysis that cannot be remedied. Specifically, cells should not have unpleasant odor, should be consistent in color, do not readily form clumps or settle when taken out of the shaker, and should be seen as turgid, consistently-sized oval spheroids under a conventional light microscope. Sick cells tend to be small and clump together, and some protease-deficient strains seems to have a tendency to look sick under the microscope. Ready-to-harvest cells were pelleted (1,500 g, 10 min), resuspended in wash buffer (50 mM 2-amino-2hydroxymethyl-propane-1,3-diol [Tris], 150 mM NaCl, pH 7.4), and then pelleted again. Cell pellets were stored at -80 ºC and typically used within 2 weeks. Longer storage time in the freezer causes quality issues, such as difficulty obtaining adequate amount of protein, or protein not binding to StrepTrap columns efficiently.

Additional notes to protein expression in *P. pastoris*: the growth conditions and requirements for a particular clone, and/or type of protein expressed, can vary. Every material used throughout the culturing process must be examined for troubleshooting. As an example, yeast extract and casein peptone from certain vendors work well for all clones and strains, while other vendors only allow expression of certain clones and strains.

Protein Expression and Purification

Frozen *P. pastoris* pellets were thawed and resuspended in lysis buffer (300 mM KCl, 50 mM Tris, pH 7.4 at room temperature) at a ratio of 1:4 cell weight to buffer volume ratio. The cell mixture was supplemented by a protease inhibitor cocktail tablet (Roche Pharmaceuticals) and was stirred until homogenized. The mixture was passed through an M-110PS microfluidizer (Microfluidics) at 30,000 psi for a total of four passes. Insoluble material was pelleted by centrifugation at 25,000 g for 30 min at 4 ºC. Supernatant was pooled and a final concentration

of 1.5% DDM (n-Dodecyl-β-D-Maltopyranoside, Anatrace) was applied to the mixture to extract membrane proteins while stirring at 4 ºC overnight. Imidazole was then added to final concentration of 10 mM, and the mixture was clarified by centrifugation (100,000 g, 10 ºC for 30 min). The supernatant was then loaded onto an XK16/20 column (GE Healthcare) packed with 15mL of Ni-NTA Agarose beads (Qiagen) pre-equilibrated by buffer A (150 mM KCl, 30 mM Tris, 10 mM imidazole, 10% glycerol and 0.025% DDM, pH 7.6 at room temperature). After the solution was passed through the column, 15 mL of wash buffer consisting of buffer A supplemented with an additional 0.5% DDM was applied. The column was then exchanged into several column volumes of buffer A or until a steady baseline for 280 nm absorbance was established. The protein was eluted with 40 mL of buffer B (150 mM KCl, 30 mM Tris, 300 mM imidazole, 10% glycerol and 0.022% DDM, pH 7.6 at room temperature). Peak fractions were pooled, then loaded onto a HiPrep 26/10 desalting column (GE Healthcare) pre-equilibrated with Buffer C (150 mM KCl, 30 mM Tris, 10 mM β-mercaptoethanol (BME), 10% Glycerol and 0.022% DDM, pH 7.5 at room temperature). Peak fractions were pooled and then loaded onto two 5-mL StrepTrap HP Columns (GE Healthcare) connected in tandem pre-equilibrated in buffer C. Buffer D (150 mM KCl, 30 mM Tris, 10 mM BME, 4 mM d-desthiobiotin, 10% glycerol and 0.022% DDM, pH 7.5 at room temperature) was applied to elute recombinant protein from the StrepTrap HP Columns. Peak fractions were pooled and once again loaded onto a HiPrep 26/10 desalting column pre-equilibrated with Buffer C to remove d-desthiobiotin. This step is vital to the stability of the cleaved protein in subsequent purification steps. Peak fractions were pooled before adding His-tagged TEV protease produced in-house [94]. The mixture was incubated overnight at 9 ºC and then filtered through a 0.45 μm syringe filter (Pall Corporations). The protein solution was loaded onto a 5-mL HisTrap HP column (GE Healthcare) equilibrated

in buffer E (150 mM KCl, 30 mM Tris, 25 mM imidazole, 10% glycerol and 0.022% DDM, pH 7.6 at room temperature). Flow-through containing the untagged GIRK2 was collected and concentrated using a 100,000 MWCO concentrator (Millipore) to roughly 2 mg/ml as determined by UV absorbance (with coefficient of 1 Abs = 1 mg/mL). The protein was flash-frozen in liquid nitrogen, stored at -80 ºC, and typically used within two weeks. These steps should consistently generate stable protein stock prior to the final polishing step for mass spectrometry analysis of GIRK2.

GIRK2 Polishing for Native Mass Spectrometry Studies.

About ~1 mg of purified GIRK2 protein solution was thawed and added to buffer F (150 mM KCl, 50 mM NaCl, 30 mM Tris, 10 mM BME, 1 mM DTT [1,4-dithiothreitol], 10% glycerol, 15 mM DHPC [1,2-diheptanoyl-sn-glycero-3-phosphocholine] and 0.022% DDM, pH 7.5 at room temperature). The ratio of protein solution to buffer F added is 1:8 by volume and the solutions were kept at 15 ºC before mixing. The mixture was immediately concentrated in a 100,000 MWCO concentrator at 3,000 g and 15 ºC for 3 minutes, and the mixture was manually re-suspended with a pipette. This process was repeated until 1 mL of solution remain to avoid precipitation of the protein. 10 mL of buffer C was added to the concentrator and the sample slowly concentrated to a final volume of 500 μL with repeated resuspension of the solution in the concentrator every 3 minutes to minimize aggregation. The mixture was then filtered through a 0.22 μm spin-filter (Millipore) before being injected into a Superdex 200GL 10/300 (GE Healthcare) column equilibrated in buffer G (150 mM KCl, 50 mM NaCl, 30 mM Tris, 10% glycerol, 0.07% $C_{10}E_5$ (decylpentaglycol, Anatrace), and pH 7.4 at room temperature). Peak fractions containing delipidated GIRK2 were pooled and concentrated in a 100,000 MWCO

concentrator until 50 μL total volume was reached. Concentrated proteins were either flash-frozen in liquid nitrogen and stored at -80 ºC, or used directly by exchanging into MS buffer (100 mM ammonium formate, 0.065% $C_{10}E_5$, and pH 7.2 at room temperature) using a centrifugal buffer exchange device (MicroBio-Spin6, Bio-Rad) following manufacture's protocol. Ammonium formate is used instead of the typical ammonium acetate due to GIRK2 having slightly better shelf-life in this buffer. For convenience, the sample in MS buffer was aliquoted into 2 μL fractions, flash-frozen in liquid nitrogen and stored at -80 ºC until used for experiments. During experiments, frozen aliquots of proteins were stored on dry ice until used for MS measurements. Notably, there should be very little observable difference in mass-spectral quality after a single freeze-thaw of GIRK2 proteins up until this point of this purification regime.

Preparation of Phospholipids and Other Ligands for MS Binding Studies

Phospholipid stock solutions were aliquoted. Chloroform was removed from the phospholipid ampoules, which were pre-aliquoted by Avanti Polar Lipid, by gentle nitrogen gas flow and then by desiccation overnight. For lipids purchased in powder form, chloroform was added, and the solution was transferred to a new glass vial and dried as described above. The dried lipid films were solubilized in the MS buffer with the exception of PIPs, where they were solubilized in water supplemented with 10mM bME. This is done to accommodate the making of multiple working stocks of PIPs in various buffers, and conserve material usage. Lipid concentrations were calculated directly from the weight of each aliquots in individual vials. The molar ratio of wild-type or R201A GIRK2 to phospholipids was held constant at a ratio of 1:6. Protein aliquots were kept at -80 ºC until immediately before usage, whereby they are mixed

with lipid solutions at a 1:1 volume ratio. Specifically, GIRK2 and lipid mixtures were held at a final concentration of about 500 nM and 3 μM, respectively. The R201A GIRK2 and lipid mixtures were at a final concentration of about 825 nM and 5 μM, respectively. These protein-lipid mixtures were allowed to incubate for 1 minute at room temperature before loading into a gold-coated glass capillary tip produced in-house as previously described [27]. Briefly, borosilicate glass capillaries (Sutter Instruments BF150-86-10) were pulled into emitters with sharp tips by using the P1000 micropipette puller (Sutter Instruments), then subsequently coated with gold using a sputter coater (Leica EM ACE600). We have found that longer incubation time does not change the mole fractions of apo and lipid-bound proteins. These findings are in agreement with our previous studies on AmtB and lipid complexes [39].

Ivermectin (Alfa Aesar) was solubilized in DMSO and/or 100% ethanol, and dilutions made in MS buffer. No noticeable precipitation of ivermectin was observed after dilution in MS buffer until a final concentration of 2mM in 20% DMSO or 5% ethanol, 3% DMSO is reached. This sample was mixed with GIRK2 in a 1:5 ratio by volume of ivermectin to GIRK2. Tertiapin Q (TPNQ, Alomone Labs) was diluted directly in MS buffer to 100 μM or lower, and mixed with GIRK2 in a 1:1 ratio by volume.

Native Mass Spectrometry (MS) and Data Analysis

A Synapt G1 HDMS instrument (Waters Corporation) with a 32k RF generator was used for most of the data collected. Instrument parameters were tuned to maximize ion intensity and simultaneously preserve the native-like state of GIRK2. The capillary voltage was set to1.75 kV, sampling cone voltage at 200 V, extractor cone voltage at 10 V and argon flow rate at 7 mL/min

(5.2 x 10^{-2} mbar). The T-wave settings for trap (300 ms and 1/1.0 V), IMS (300 ms and 1/18 V) and transfer (100 ms and 1/10 V), source temperature (90 ºC) and trap bias (35 V) were also optimized. Trap and Transfer Collision Voltage were set to 100 V and 60 V, respectively, unless otherwise noted. Ion mobility mass spectrometry data were processed using the software program Pulsar [35] and de-convoluted using UniDec [95] followed by converting intensities of GIRK2 and PIP-GIRK2 species to mole fractions as described previously [39].

High-resolution MS spectra were collected using an Exactive Plus with extended mass range (EMR) from Thermo Scientific. Samples were analyzed using both the original instrument and a modified reverse entry ion source (REIS) coupled to the HCD cell of the Orbitrap [96]. Gold-coated capillaries described above were loaded with sample. Operating conditions of the REIS were described in detail previously; briefly, ions are generated by nano-ESI, focused with a RF ion funnel, and transferred to the HCD cell by an octupole ion guide. All mass spectra were collected with 10 µscans at 17 500 mass resolution with an ion injection time of 200 ms. Collision energies of 20 eV in-source CID and 70 HCD collision energy for normal operating conditions and 110 HCD collision energy for REIS. These energies were chosen to effectively desolvate and strip detergents while minimizing perturbations to protein-lipid and subunit interactions. MS data from the Exactive Plus EMR is analyzed and mass-species assigned using UniDec [95].

Results and Discussion

GIRK2 Sample Optimization for Native Mass Spectrometry

We initially performed protein expression and purification for GIRK2 following established methods used for crystallographic studies of GIRK2 [77, 78], and recorded a mass spectrum of GIRK2 solubilized in dodecylmaltoside (DDM) detergent micelles. High-energy instrument settings were necessary to obtain an interpretable mass spectrum on a Waters Synapt G1 instrument (Fig 7A and Fig 8A). The mass spectral peak group with the highest signal intensity correspond to the tetrameric channel (~8000 *m/z* for Fig 7, ~6000 *m/z* for Fig 8A,B). Significant adducts remain bound, even under this high-energy regime, corresponding to a host of small molecules contaminants, which we suspect are co-purified lipids. We then used a detergent screening approach [9] to identify conditions that remove the co-purified contaminants from the complex (Fig 7). From this exhaustive screen of detergents performed at different steps in the purification process, including mixtures of detergents, no conditions were found to effectively remove all of the bound contaminants while maintaining protein solubility. We then explored lipids with detergent-like properties and found the short-chain phospholipid DHPC (1,2-diheptanoyl-sn-glycero-3-phosphocholine) to be the most effective at removing adducts while minimizing protein aggregation. The mass spectrum of GIRK2 in DDM after DHPC treatment had no lipid adducts even under moderate instrument settings (Fig 8B). Although the mass spectrum is resolved, it is difficult to preserve native-like structure using DDM, a non-charge reducing detergent, as evident by broad arrival time distributions and dissociation of the complex (Fig 8B and 9A). Similar observations have been made for other membrane proteins [22, 27]. Therefore, we exchanged GIRK2 into buffer containing the charge-reducing detergent

$C_{10}E_5$ (decylpentaglycol) (Fig 7C). The mass spectrum of this sample is well-resolved and the ion mobility (IM) measurements, which report on the rotationally averaged collision cross-section, indicate compact, native-like arrival times for half of the charge states under the optimized instrument settings (Fig 7C and 9B). The measured mass agrees highly with the calculated mass (Table 1). The $C_{10}E_5$ detergent micelle requires more energy to release from the protein than the commonly used C_8E_4 detergent, providing an explanation for the partial activation of the higher charge states seen in Fig 9B [22]. Notably, the sample following established methods in DDM under the same instrument conditions used for the optimized sample in $C_{10}E_5$ was largely a hump with some poorly resolved mass spectral peaks observed (Fig 10A). Moreover, the $C_{10}E_5$ detergent reduces enough charge such that no dissociation of the complex is observed even at the highest energy regime (Fig 10B), which is in accord with other charge-reduced membrane protein studies performed previously [22, 27, 97].

We also acquired data on a higher mass resolution Orbitrap mass spectrometer [46] equipped with a custom reverse-entry ion source (REIS-Orbitrap) [98, 99] that yielded sharp mass spectral peaks with addition of mass as small as 80 ± 17 Da resolved (Fig 8D). As the 80 Da addition in mass could be a covalent modification, we prepared a denatured sample of GIRK2 following a method recently reported by Campuzano and co-workers [100]. The mass spectrum of the denatured sample recorded on the Orbitrap mass spectrometer revealed a predominant denatured mass of 38,939.65 Da (Fig 11), which is within 2.20 Da of the calculated mass of GIRK2 with the initiating methionine removed. Removal of the first residue by methionine aminopeptidase is not an uncommon post-translational modification [101, 102]. Moreover, a denatured mass consistent with one phosphorylation of GIRK2 was also measured and accounts

for a small fraction of the total signal. This percentage of phosphorylation is consistent with the decrease in intensity of one and multiple phosphorylation events within the tetrameric complex. We then performed a tryptic peptide analysis to confirm phosphorylation and identify site(s) of the covalent modification. We obtained a sequence coverage of 52% and a number of peptides having only a single phosphorylation were identified (Fig 12A). Of those, four phosphorylated residues mapped to surface exposed regions of the cytoplasmic domain near the C-terminus (Fig 12B). Two serine residues that are part of the linker region between GIRK2 and the TEV protease cleavage site of the expression construct were unexpectedly both found to be singly phosphorylated.

GIRK2 Interactions With the Peptide Antagonist TPNQ and the Drug Imvermectin

Given the high-quality samples of GIRK2 revealed by MS above, we next explored if we could resolve binding of small molecules, such as toxins and drugs. The first molecule we considered was tertiapin, a 21 amino acid peptide isolated from honey bee venom and a potent inhibitor of GIRK2 and other IRKs [73]. We used the oxidation resistant form of tertiapin where Met13 has been mutated to Q (TPNQ) with a molecular weight of 2452 Da [103]. The mass spectrum of a mixture of TPNQ to GIRK2 at a 6:1 molar ratio in the detergent $C_{10}E_5$ revealed direct binding of one TPNQ molecule (Fig 13A). Interestingly, the arrival time distributions differed significantly for apo and TPNQ bound GIRK2 (Fig 13B). For example, the 17^+ charge state had a more compact conformer for GIRK2•TPNQ whereas the apo species was predominantly an extended, activated conformer of the protein (Fig 13B). These results prompted us to perform a collision induced unfolding (CIU) experiment where gas-phase unfolding is monitored by ion mobility, an approach that has been successfully employed for

soluble [32] and membrane protein complexes [104]. The ion mobility profiles begin with a native-like arrival time distribution where the applied instrument energy regimes are sufficient to remove detergent micelles but insufficient to perturb protein structure (Fig 13C and Fig 14), in similar ways to other membrane protein complexes was studied [27]. As collision energy is increased, the arrival time distribution transitions to a partially unfolded state (Fig 13C and Fig 14) at 145 electron volts (eV) for the 17^+ charge state of GIRK2. Since charge-reducing detergents are used, there is no dissociation of GIRK2 and GIRK2•TPNQ complexes even at the highest collision energies. Applying algorithms to quantify transitions in CIU profiles [27, 35] we calculated an average stabilization for the binding of TPNQ to GIRK2 of 640 and 637 eV for the 17^+ and 18^+ charge states, respectively (Fig 13D). In summary, CIU experiments reveal that TPNQ bound GIRK2 significantly stabilizes the channel with an increased resistance to the gas-phase unfolding forces.

The second small molecule we studied was ivermectin, a hydrophobic drug molecule identified in functional assays to activate GIRK2 channels [76, 105]. The drug has a molecular weight of 875 Da that is comparable to the mass of PIPs (Fig 15A). Unlike TPNQ, we observed no binding of ivermectin to the channel under our experimental conditions even at concentrations as high as 300 μM (Fig 15B), which is three-fold higher than values used in previous studies. Since functional studies report a $PI(4,5)P_2$-dependent but $G_{\beta\gamma}$-independent activation of GIRK2 channels by ivermectin, we incubated GIRK2 with a mixture of ivermectin and a $PI(4,5)P_2$ with 18:0-20:4 tails ($PI(4,5)P_2$-sa) at 1:100:6 molar ratio, respectively. The mass spectrum for these mixtures compared to the mass spectrum to a sample free of ivermectin was indistinguishable, implying no direct binding of the drug (Fig 15C, D). Additionally, no significant mass spectral

peak broadening or shift was observed in the presence of the drug. These results demonstrate the ability of our mass spectrometry approach to identify molecules that are direct binders.

GIRK2 Binding with Phospholipids

To probe the selectivity of PIPs we incubated GIRK2 with a six-fold molar excess of phosphatidylinositol-4-phosphate (PI(4)P), phosphatidylinositol-3,4-bisphosphate (PI(3,4)P_2), PI(4,5)P_2 with dioleoyl acyl chains (18:1-18:1, do), dioctanoyl (8:0-8:0, d8) PI(4,5)P_2, 1-stearoyl-2-arachidonoyl (18:0-20:4, sa) PI(4,5)P_2-sa, and phosphatidylinositol-3,4,5-triphosphate (PI(3,4,5)P_3-sa) (see Table 2 for abbreviations). Native mass spectra for GIRK2 incubated with PIPs revealed binding of up to four molecules including peaks corresponding to the apo channel (Fig 16). As the mass spectral peaks were broad, we introduced the sample into the REIS-Orbitrap and obtained higher resolution mass spectra with slightly less lipid-bound fractional abundances (Fig 16B). We observed peak splitting in the presence of PI(4,5)P_2-d8 corresponding to 90 ± 40 Da. After deconvoluting the mass spectra [95] and extracting mole fraction data, PI(4,5)P_2-do and PI(3,4)P_2-do bound with similar abundance to PI(4,5)P_2-d8 (Fig 14C). In the case of PI(4)P-do, which contains one less phosphate group, the overall abundance of bound lipid was significantly reduced as evident by an increase in the fractional abundance of apo GIRK2. PI(3,4,5)P_3-sa, a lipid with three phosphates groups on the inositol head group, also showed a reduction in binding as indicated by a higher fractional abundance of the apo channel compared to PI(4)P-do. The mass spectrum for PI(4,5)P_2-sa, a lipid with similar acyl chains as PI(3,4,5)P_3-sa, had comparable binding to the other acyl variants of PI(4,5)P_2 studied. These data indicate GIRK2 selectively binds PI(3,4)P_2 and PI(4,5)P_2 with roughly equivalent affinity while displaying a lack of sensitivity toward acyl chain length.

We next examined the data to compare the gas-phase stabilization imparted by lipids and TPNQ. The ATD for PIP_{1-4} bound to GIRK2 acquired under optimized instrument settings did not preserve the native-like distribution for the $17^+/18^+$ ions when compared to GIRK2 bound to TPNQ (Fig 17A, B). We then performed CIU on the apo and PI(4,5)P_2-do bound to GIRK2 and found that a modest stabilization, between 150 and 200 eV, was achieved when four PI(4,5)P_2-do were bound to GIRK2 (Fig 17E). PIP binding clearly stabilizes the channel but to a lesser extent than TPNQ.

To compare the affinity of PIPs to other phospholipids we considered binding of phosphatidylinositol (PI) with do-type acyl chains (DOPI), phosphatidylcholine (PC) and phosphatidylethanolamine (PE) with 1-palmitoyl-2-oleoyl (16:0–18:1, PO) acyl chains at the same molar ratio used for the PIP binding studies described above (Fig 16C). In the case of DOPI, a precursor for PIPs, there was a significant reduction in binding and only up to three lipid binding events were observed compared to four PIPs bound. For POPE, a maximum of two lipids were bound, with 66% of the signal corresponding to apo GIRK2. POPC differs from POPE by three additional methyl groups on the choline headgroup and was the weakest binder of the lipids studied. Other studies have reported the sensitivity of Kir2 to PI(4,5)P2 can be modulated by anionic lipids [71], we explored this possibility with GIRK2 and incubated the channel with four molar equivalents of PI(4,5)P2-do and POPG (Fig 18). The mass spectrum revealed no significant differences in binding of PI(4,5)P2-do compared to samples lacking POPG, which would be expected for competitive binding or positive allosteric modulation [91]. Taken together, GIRK2 binds PIPs with much higher affinity compared to other phospholipids.

GIRK2 Mutant Binding Phospholipids

The GIRK2^{R201A} mutant, a channel with a slightly shifted cytoplasmic domain rotation compared to the wild type, is reported to gate by PIPs independently of $G_{\beta\gamma}$ (Fig 19). Similar lipid binding experiments done for the wild type channel was performed for this mutant (Fig 20). The most abundant binding was observed for PI(4,5)P_2-d8 and binding was similar for PI(4,5)P_2-do, and PI(4,5)P_2-sa (Fig 20C). In the case of PI(3,4)P_2-do, a significant reduction in binding affinity was observed relative to wild-type GIRK2. The mass spectrum for PI(4,5)P_2 and PI(3,4,5)P_3 revealed comparable binding affinity to the wild-type protein. The mutant channel also displayed an overall increase in binding affinity towards DOPI, POPC and POPE compared to wild-type GIRK2. Taken together, GIRK2^{R201A} displays a greater selectivity towards PIP isoforms with head group phosphorylation at the 4 and 5 positions and reduced affinity towards the other PIPs.

In a similar fashion to the wild-type channel, we examined the GIRK and GIRK^{R201A} data to compare the gas-phase stabilization imparted by lipids and TPNQ. GIRK^{R201A} bound to TPNQ was significantly stabilized to a level that was comparable to the wild-type protein (Fig 21, Fig 22). Like the wild-type protein, PIPs had similar stabilization to the mutant channel under the optimized instrument settings used. Interestingly, when we incubated GIRK2, TPNQ and PIP(4,5)P2-d8 at a molar ratio of 1:6:6, respectively, all 17+ species with TPNQ bound show a large degree of stabilization with faster, more compact arrival times (Fig 23). Lastly, we compared charge states that represent partially unfolded and native-like states (the 21^+ and 16^+, respectively) (Fig 24). Significant dissociation was observed for DOPI, POPC, and POPE at higher charge states (Fig 24B-C). In contrast, the abundance of PIPs bound were nearly identical

between the two charge states suggesting that GIRK2 specifically bind PIPs. This phenomenon is supported by observation of increased binding affinity for PIPs in relation to other phospholipid species.

Discussion of Results

In order for a drug to be efficacious it must directly bind and modulate the function of the target protein [106, 107]. Here, we demonstrate the utility of native mass spectrometry to monitor direct binding of small molecules to GIRK2. The high-quality samples produced was instrumental in enabling the first high-resolution native mass measurements of a eukaryotic ion channel with the striking ability to resolve adducts as small as 80 Da on the intact 156 kDa tetrameric complex. These adducts were further confirmed using traditional top-down and bottom-up proteomic approaches to be phosphorylation of GIRK2 on residues previously unreported. The covalent modifications mapped to surface exposed residues located in the CTD and, unexpectedly, to both serine residues within the linker region of the expression construct. Removal of the serine residues in the linker region will undoubtedly improve protein homogeneity. For GIRK2, the reported phosphorylation events that have roles in protein trafficking and modulating activity are located in the N-terminal region [54, 108-110]. Although the new GIRK2 phosphorylation sites we identified here warrant further study, it is important to highlight that a native mass spectrum can provide insight in protein modifications that may go undetected. The methods in optimizing the sample quality to enable these measurements are numerous and summarized to highlight key points (Fig 25). Taken together, our mass spectrometry results and methods provide the foundation for future studies to not only improve sample quality but also detect post-translational modifications.

The optimized instrument settings for GIRK2 resulted in a balance of compact, native-like arrival times for half of the charge states as determined by IM. Here, we have avoided interpreting activated ions and only deconvoluted regions of the mass spectrum corresponding to ions with native-like arrival times. One potential issue this technique often faces is with regard to whether the electrostatic and hydrophobic interactions of the complex can be purturbed in the gas-phase. However, in our previous reports [39, 88] and from the Klassen group [89], binding thermodynamics for soluble protein-ligand, membrane protein-protein, and membrane protein-lipid interactions determined by native MS are in direct agreement with surface plasmon resonance and isothermal titration calorimetry, which are gold-standards for solution-phase measurements. The fact that similar equilibrium constants and thermodynamic parameters to solution measurements can be determined by native MS suggest the altered electrostatic and hydrophobic interactions in the gas-phase are negligible. Although corroborating our lipid binding data with another assay would be a logical follow-up study, our existing ion mobility measurements can help us minimize potential gas-phase artifacts due to instrument energy activation. We can extract mole fraction lipid binding data from only ions with compact, native-like arrival times, and interpret the data with confidence.

Native ion mobility mass spectrometry not only can monitor direct binding events but probe membrane protein stability in complex with small molecules. The IM-MS data for GIRK bound to TPNQ provide compelling evidence that the toxin binds and significantly stabilizes the channel. Increased protein stabilization upon ligand binding, including membrane protein-lipid interactions, has been well characterized by ion mobility [27, 32]. Notably, the gas-phase stabilization observed here for GIRK2•TPNQ is over six-fold more stabilizing compared to

values reported for membrane protein lipid interactions for a single binding event [27]. In the case of the recently reported GIRK2 activator ivermectin, no direct binding was observed. The absence of ivermectin binding to GIRK2 using our native IM-MS approach suggests the drug molecule may bind weakly and/or require a lipid bilayer to support binding. Another possibility for no apparent binding is the energy regime required to release the protein from the detergent micelle is too high and may dissociate the bound drug.

Our direct mass measurements of the GIRK2-lipid complexes reveal that both GIRK2 and GIRK2^{R201A} display distinct specificity for the phosphorylation pattern of the inositol head group. More specifically, GIRK2 and GIRK2^{R201A} both have high affinity for PI(4,5)P_2 whereas the wild-type channel also has comparable affinity for PI(3,4)P_2. Although the majority of assays use predominantly PI(4,5)P_2 to activate GIRK2, our results are largely in agreement with functional studies for other GIRKs, which observed head group selectivity compared to other IRKs [68, 71, 79]. The slight differences between our direct binding measurements and channel activation represents an interesting question as to the correlation between PIP binding events and gating. Moreover, the acyl chain variations among the PIPs explored here show insignificant differences in preference that is in contrast with functional studies that reported differences in acyl chains lengths for GIRK1/4 [68]. Although GIRK2 is in the same subfamily as GIRK1/4, the data suggests these two channels have a different selectivity towards the lipid tails of PIPs. In summary, GIRK2 lipid selectivity is largely determined by head group phosphorylation pattern of the PIPs, and not necessarily through acyl chain length.

Mass spectrometry results also reveal that GIRK2 and GIRK2^{R201A} bind PIPs cooperatively and with much higher affinity than highly abundant phospholipids in the plasma membrane [111]. GIRK2 binds DOPI, POPC, and POPE with reduced binding affinity compared PIPs. At equimolar concentrations, up to three lipid binding events to GIRK2 were observed for DOPI, POPC, and POPE whereas four PIPs can be seen bound. The much higher binding affinity of GIRK2 towards PIPs provides evidence for how these channels can bind PIPs that are found in low abundance compared to bulk lipids in the plasma membrane.

Allosteric modulation of protein function by binding of molecules at remote sites is an important biological phenomenon [112-114]. Here, GIRK2^{R201A} allowed us to explore lipid binding to a channel that induces a rotation in the CTD, similarly to $G_{\beta\gamma}$-activated state of GIRK2 [77]. The mutant was primarily used because the biochemical isolation of the GIRK2•$G_{\beta\gamma}$ complex in detergent solutions has so far been unsuccessful [78]. Early studies indicate GIRK interactions with PI(4,5)P_2 are weak and that there is an increase in relative affinity for the $G_{\beta\gamma}$-activated channel [61, 115]. However, our data suggest that rotation of the GIRK2 CTD when bound to $G_{\beta\gamma}$, as mimicked here by GIRK2^{R201A}, does not enhance or decrease the binding affinity towards PI(4,5)P_2. Rather, rotation of the CTD allosterically modulates remote PIP binding sites, tuning the channel by reducing the binding affinity for PIP isoforms known to weakly or not activate GIRKs. Our findings are in-line with recent MS studies suggesting membrane protein-lipid interactions can allosterically modulate interactions with regulatory and signaling proteins [88, 116]. Although the R201A CTD rotation is greater than the GIRK2•$G_{\beta\gamma}$ complex, it is reasonable to suggest that rotation of the CTD allosterically tunes the selectivity of the channel towards PIPs.

CHAPTER IV

SUMMARY AND CONCLUSIONS

Native ion-mobility mass spectrometry (IM-MS) demonstrated individual protein-ligand binding details can be quantitatively analyzed. The ammonium channel AmtB was used to help establish rigorous methods for IM-MS studies for more complex eukaryotic membrane complexes, such as the inward rectifying potassium (IRK) channels from mammals. In this dissertation, IM-MS was used to monitor direct binding of lipids and a toxin to a mouse G-protein-gated IRK (GIRK2). This study revealed direct yet unprecedented details about the channel that are conventionally difficult to access, such as how the signaling lipids, phosphoinositides (PIPs), may selectively bind GIRK2 with much higher affinity over other phospholipids. In addition, using the R201A mutant channel which exhibits a cytoplasmic domain (CTD) rotation similar to the $G_{\beta\gamma}$-activated state, it showed that an altered structure can allosterically modulate binding selectivity towards PIPs at a distant site. The level of detail from mass measurements of an optimized membrane channel has also guided us to observe previously unreported phosphorylation events to GIRK2's C-terminus. Ion mobility measurements, coupled to native MS, also provides useful information on the structural consequences of non-covalent interactions between a protein and its ligand(s). Going forward, the continued improvement in both sample preparation and native MS technology such as IM resolution will allow us to decipher further details of disease-related membrane proteins such as GIRK2. Application of high-resolution, native IM-MS techniques will provide a new window into the structural and biophysical details of complex cellular machinery to greater depth.

REFERENCES

[1] S. J. Singer and G. L. Nicolson, "The fluid mosaic model of the structure of cell membranes," *Science,* vol. 175, pp. 720-31, Feb 18 1972.

[2] A. G. Lee, "Biological membranes: the importance of molecular detail," *Trends Biochem Sci,* vol. 36, pp. 493-500, Sep 2011.

[3] F. X. Contreras, A. M. Ernst, F. Wieland, and B. Brugger, "Specificity of intramembrane protein-lipid interactions," *Cold Spring Harb Perspect Biol,* vol. 3, Jun 2011.

[4] S. B. Long, X. Tao, E. B. Campbell, and R. MacKinnon, "Atomic structure of a voltage-dependent K+ channel in a lipid membrane-like environment," *Nature,* vol. 450, pp. 376-82, Nov 15 2007.

[5] J. P. Overington, B. Al-Lazikani, and A. L. Hopkins, "How many drug targets are there?," *Nat Rev Drug Discov,* vol. 5, pp. 993-6, Dec 2006.

[6] M. A. Yildirim, K. I. Goh, M. E. Cusick, A. L. Barabasi, and M. Vidal, "Drug-target network," *Nat Biotechnol,* vol. 25, pp. 1119-26, Oct 2007.

[7] B. T. Ruotolo, K. Giles, I. Campuzano, A. M. Sandercock, R. H. Bateman, and C. V. Robinson, "Evidence for macromolecular protein rings in the absence of bulk water," *Science,* vol. 310, pp. 1658-61, Dec 9 2005.

[8] A. B. Kanu, P. Dwivedi, M. Tam, L. Matz, and H. H. Hill, Jr., "Ion mobility-mass spectrometry," *J Mass Spectrom,* vol. 43, pp. 1-22, Jan 2008.

[9] A. Laganowsky, E. Reading, J. T. Hopper, and C. V. Robinson, "Mass spectrometry of intact membrane protein complexes," *Nat. Protoc.,* vol. 8, pp. 639-51, Apr 2013.

[10] H. Hernandez and C. V. Robinson, "Determining the stoichiometry and interactions of macromolecular assemblies from mass spectrometry," *Nat Protoc,* vol. 2, pp. 715-26, 2007.

[11] J. L. Benesch and C. V. Robinson, "Mass spectrometry of macromolecular assemblies: preservation and dissociation," *Curr Opin Struct Biol,* vol. 16, pp. 245-51, Apr 2006.

[12] J. A. Loo, "Studying noncovalent protein complexes by electrospray ionization mass spectrometry," *Mass Spectrom Rev,* vol. 16, pp. 1-23, Jan-Feb 1997.

[13] K. Lorenzen and E. van Duijn, "Native mass spectrometry as a tool in structural biology," *Curr Protoc Protein Sci,* vol. Chapter 17, p. Unit17 12, Nov 2010.

[14] L. Pedro and R. J. Quinn, "Native Mass Spectrometry in Fragment-Based Drug Discovery," *Molecules,* vol. 21, 2016.

[15] D. R. Goodlelt, R. R. Ogorzalek Loo, J. A. Loo, J. H. Wahl, H. R. Udseth, and R. D. Smith, "A study of the thermal denaturation of ribonuclease S by electrospray ionization mass spectrometry," *J Am Soc Mass Spectrom,* vol. 5, pp. 614-22, Jul 1994.

[16] C. V. Robinson, E. W. Chung, B. B. Kragelund, J. Knudsen, R. T. Aplin, F. M. Poulsen, *et al.*, "Probing the Nature of Noncovalent Interactions by Mass Spectrometry. A Study of Protein−CoA Ligand Binding and Assembly," *Journal of the American Chemical Society,* vol. 118, pp. 8646-8653, 1996/01/01 1996.

[17] S. G. Penn, H. Fei, M. Kirk Green, and C. B. Lebrilla, "The use of heated capillary dissociation and collision-induced dissociation to determine the strength of noncovalent bonding interactions in gas-phase peptide-cyclodextrin complexes," *Journal of the American Society for Mass Spectrometry,* vol. 8, pp. 244-252, 1997/03/01 1997.

[18] F. He, J. Ramirez, B. A. Garcia, and C. B. Lebrilla, "Differentially heated capillary for thermal dissociation of noncovalently bound complexes produced by electrospray ionization1," *International Journal of Mass Spectrometry,* vol. 182–183, pp. 261-273, 3/1/ 1999.

[19] V. Gabelica, F. Rosu, C. Houssier, and E. De Pauw, "Gas phase thermal denaturation of an oligonucleotide duplex and its complexes with minor groove binders," *Rapid Commun Mass Spectrom,* vol. 14, pp. 464-7, 2000.

[20] J. L. Lippens, J. B. Mangrum, W. McIntyre, B. Redick, and D. Fabris, "A simple heated-capillary modification improves the analysis of non-covalent complexes by Z-spray electrospray ionization," *Rapid Commun Mass Spectrom,* vol. 30, pp. 773-83, Mar 30 2016.

[21] N. P. Barrera, N. Di Bartolo, P. J. Booth, and C. V. Robinson, "Micelles protect membrane complexes from solution to vacuum," *Science,* vol. 321, pp. 243-6, Jul 11 2008.

[22] E. Reading, I. Liko, T. M. Allison, J. L. Benesch, A. Laganowsky, and C. V. Robinson, "The role of the detergent micelle in preserving the structure of membrane proteins in the gas phase," *Angew Chem Int Ed Engl,* vol. 54, pp. 4577-81, Apr 7 2015.

[23] N. G. Housden, J. T. Hopper, N. Lukoyanova, D. Rodriguez-Larrea, J. A. Wojdyla, A. Klein, *et al.,* "Intrinsically disordered protein threads through the bacterial outer-membrane porin OmpF," *Science,* vol. 340, pp. 1570-4, Jun 28 2013.

[24] E. Reading, I. Liko, T. M. Allison, J. L. Benesch, A. Laganowsky, and C. V. Robinson, "The role of the detergent micelle in preserving the structure of membrane proteins in the gas phase," *Angew. Chem. Int. Ed. ,* vol. 54, pp. 4577-81, Apr 7 2015.

[25] M. Landreh, I. Liko, P. Uzdavinys, M. Coincon, J. T. Hopper, D. Drew, *et al.*, "Controlling release, unfolding and dissociation of membrane protein complexes in the gas phase through collisional cooling," *Chem Commun (Camb),* vol. 51, pp. 15582-4, Nov 4 2015.

[26] A. J. Borysik, D. J. Hewitt, and C. V. Robinson, "Detergent release prolongs the lifetime of native-like membrane protein conformations in the gas-phase," *J Am Chem Soc,* vol. 135, pp. 6078-83, Apr 24 2013.

[27] A. Laganowsky, E. Reading, T. M. Allison, M. B. Ulmschneider, M. T. Degiacomi, A. J. Baldwin, *et al.*, "Membrane proteins bind lipids selectively to modulate their structure and function," *Nature,* vol. 510, pp. 172-5, Jun 5 2014.

[28] A. Konijnenberg, D. Yilmaz, H. I. Ingolfsson, A. Dimitrova, S. J. Marrink, Z. Li, *et al.*, "Global structural changes of an ion channel during its gating are followed by ion mobility mass spectrometry," *Proc Natl Acad Sci U S A,* vol. 111, pp. 17170-5, Dec 2 2014.

[29] B. T. Ruotolo, C. C. Tate, and D. H. Russell, "Ion mobility-mass spectrometry applied to cyclic peptide analysis: conformational preferences of gramicidin S and linear analogs in the gas phase," *J Am Soc Mass Spectrom,* vol. 15, pp. 870-8, Jun 2004.

[30] F. Zhu, S. Lee, S. J. Valentine, J. P. Reilly, and D. E. Clemmer, "Mannose7 glycan isomer characterization by IMS-MS/MS analysis," *J Am Soc Mass Spectrom,* vol. 23, pp. 2158-66, Dec 2012.

[31] B. T. Ruotolo, S. J. Hyung, P. M. Robinson, K. Giles, R. H. Bateman, and C. V. Robinson, "Ion mobility-mass spectrometry reveals long-lived, unfolded intermediates in

the dissociation of protein complexes," *Angew Chem Int Ed Engl*, vol. 46, pp. 8001-4, 2007.

[32] S. J. Hyung, C. V. Robinson, and B. T. Ruotolo, "Gas-phase unfolding and disassembly reveals stability differences in ligand-bound multiprotein complexes," *Chem Biol*, vol. 16, pp. 382-90, Apr 24 2009.

[33] L. Han, S. J. Hyung, J. J. Mayers, and B. T. Ruotolo, "Bound anions differentially stabilize multiprotein complexes in the absence of bulk solvent," *J Am Chem Soc*, vol. 133, pp. 11358-67, Jul 27 2011.

[34] J. N. Rabuck, S. J. Hyung, K. S. Ko, C. C. Fox, M. B. Soellner, and B. T. Ruotolo, "Activation state-selective kinase inhibitor assay based on ion mobility-mass spectrometry," *Anal Chem*, vol. 85, pp. 6995-7002, Aug 6 2013.

[35] T. M. Allison, E. Reading, I. Liko, A. J. Baldwin, A. Laganowsky, and C. V. Robinson, "Quantifying the stabilizing effects of protein-ligand interactions in the gas phase," *Nat Commun*, vol. 6, p. 8551, 2015.

[36] S. Yin, Y. Xie, and J. A. Loo, "Mass spectrometry of protein-ligand complexes: enhanced gas-phase stability of ribonuclease-nucleotide complexes," *J Am Soc Mass Spectrom*, vol. 19, pp. 1199-208, Aug 2008.

[37] N. F. Zinnel, P. J. Pai, and D. H. Russell, "Ion mobility-mass spectrometry (IM-MS) for top-down proteomics: increased dynamic range affords increased sequence coverage," *Anal Chem*, vol. 84, pp. 3390-7, Apr 3 2012.

[38] N. F. Zinnel and D. H. Russell, "Size-to-charge dispersion of collision-induced dissociation product ions for enhancement of structural information and product ion identification," *Anal Chem*, vol. 86, pp. 4791-8, May 20 2014.

[39] X. Cong, Y. Liu, W. Liu, X. Liang, D. H. Russell, and A. Laganowsky, "Determining Membrane Protein-Lipid Binding Thermodynamics Using Native Mass Spectrometry," *J Am Chem Soc,* vol. 138, pp. 4346-9, Apr 6 2016.

[40] S. D. Pringle, K. Giles, J. L. Wildgoose, J. P. Williams, S. E. Slade, K. Thalassinos, *et al.*, "An investigation of the mobility separation of some peptide and protein ions using a new hybrid quadrupole/travelling wave IMS/oa-ToF instrument," *International Journal of Mass Spectrometry,* vol. 261, pp. 1-12, 3/1/ 2007.

[41] R. J. Hilf and R. Dutzler, "X-ray structure of a prokaryotic pentameric ligand-gated ion channel," *Nature,* vol. 452, pp. 375-9, Mar 20 2008.

[42] T. Y. T. P. S. Chen, Huber Warner, "Microdetermination of Phosphorus," *Analytical Chemistry,* vol. 28, p. 3, 1956.

[43] C. H. F. a. Y. Subbarow, "The colorimetric determination of phosphorus," *Journal of Biological Chemistry,* vol. 66, p. 26, 1925.

[44] M. T. Marty, A. J. Baldwin, E. G. Marklund, G. K. Hochberg, J. L. Benesch, and C. V. Robinson, "Bayesian deconvolution of mass and ion mobility spectra: from binary interactions to polydisperse ensembles," *Anal. Chem.,* vol. 87, pp. 4370-6, Apr 21 2015.

[45] R. D. Smith and C. J. Barinaga, "Internal energy effects in the collision-induced dissociation of large biopolymer molecular ions produced by electrospray ionization tandem mass spectrometry of cytochrome c," *Rapid Communications in Mass Spectrometry,* vol. 4, pp. 54-57, 1990.

[46] J. Gault, J. A. Donlan, I. Liko, J. T. Hopper, K. Gupta, N. G. Housden, *et al.*, "High-resolution mass spectrometry of small molecules bound to membrane proteins," *Nat Methods,* vol. 13, pp. 333-6, Apr 2016.

[47] M. Bogdanov, W. Dowhan, and H. Vitrac, "Lipids and topological rules governing membrane protein assembly," *Biochim Biophys Acta*, vol. 1843, pp. 1475-88, Aug 2014.

[48] J. A. Poveda, A. M. Giudici, M. L. Renart, M. L. Molina, E. Montoya, A. Fernandez-Carvajal, *et al.*, "Lipid modulation of ion channels through specific binding sites," *Biochim Biophys Acta*, vol. 1838, pp. 1560-7, Jun 2014.

[49] Q. X. Jiang and T. Gonen, "The influence of lipids on voltage-gated ion channels," *Curr Opin Struct Biol*, vol. 22, pp. 529-36, Aug 2012.

[50] J. S. Brodbelt, "Ion Activation Methods for Peptides and Proteins," *Anal Chem*, vol. 88, pp. 30-51, Jan 5 2016.

[51] M. Zhou, S. Dagan, and V. H. Wysocki, "Protein subunits released by surface collisions of noncovalent complexes: nativelike compact structures revealed by ion mobility mass spectrometry," *Angewandte Chemie International Edition*, vol. 51, pp. 4336-4339, 2012.

[52] R. S. Quintyn, J. Yan, and V. H. Wysocki, "Surface-Induced Dissociation of Homotetramers with D 2 Symmetry Yields their Assembly Pathways and Characterizes the Effect of Ligand Binding," *Chemistry & biology*, vol. 22, pp. 583-592, 2015.

[53] B. C. Suh and B. Hille, "PIP2 is a necessary cofactor for ion channel function: how and why?," *Annu Rev Biophys*, vol. 37, pp. 175-95, 2008.

[54] H. Hibino, A. Inanobe, K. Furutani, S. Murakami, I. Findlay, and Y. Kurachi, "Inwardly rectifying potassium channels: their structure, function, and physiological roles," *Physiol Rev*, vol. 90, pp. 291-366, Jan 2010.

[55] B. R. Pattnaik, M. P. Asuma, R. Spott, and D. A. Pillers, "Genetic defects in the hotspot of inwardly rectifying K(+) (Kir) channels and their metabolic consequences: a review," *Mol Genet Metab*, vol. 105, pp. 64-72, Jan 2012.

[56] O. Furst, B. Mondou, and N. D'Avanzo, "Phosphoinositide regulation of inward rectifier potassium (Kir) channels," *Front Physiol,* vol. 4, p. 404, Jan 08 2014.

[57] M. Tristani-Firouzi, J. L. Jensen, M. R. Donaldson, V. Sansone, G. Meola, A. Hahn, *et al.*, "Functional and clinical characterization of KCNJ2 mutations associated with LQT7 (Andersen syndrome)," *J Clin Invest,* vol. 110, pp. 381-8, Aug 2002.

[58] C. M. Lopes, H. Zhang, T. Rohacs, T. Jin, J. Yang, and D. E. Logothetis, "Alterations in conserved Kir channel-PIP2 interactions underlie channelopathies," *Neuron,* vol. 34, pp. 933-44, Jun 13 2002.

[59] F. M. Ashcroft, "ATP-sensitive potassium channelopathies: focus on insulin secretion," *J Clin Invest,* vol. 115, pp. 2047-58, Aug 2005.

[60] S. McLaughlin and D. Murray, "Plasma membrane phosphoinositide organization by protein electrostatics," *Nature,* vol. 438, pp. 605-11, Dec 1 2005.

[61] C. L. Huang, S. Feng, and D. W. Hilgemann, "Direct activation of inward rectifier potassium channels by PIP2 and its stabilization by Gbetagamma," *Nature,* vol. 391, pp. 803-6, Feb 19 1998.

[62] T. Rohacs, C. M. Lopes, T. Jin, P. P. Ramdya, Z. Molnar, and D. E. Logothetis, "Specificity of activation by phosphoinositides determines lipid regulation of Kir channels," *Proc Natl Acad Sci U S A,* vol. 100, pp. 745-50, Jan 21 2003.

[63] Y. Fujiwara and Y. Kubo, "Regulation of the desensitization and ion selectivity of ATP-gated P2X2 channels by phosphoinositides," *J Physiol,* vol. 576, pp. 135-49, Oct 1 2006.

[64] S. B. Hansen, X. Tao, and R. MacKinnon, "Structural basis of PIP2 activation of the classical inward rectifier K+ channel Kir2.2," *Nature,* vol. 477, pp. 495-8, Sep 22 2011.

[65] Z. Fan and J. C. Makielski, "Phosphoinositides decrease ATP sensitivity of the cardiac ATP-sensitive K(+) channel. A molecular probe for the mechanism of ATP-sensitive inhibition," *J Gen Physiol,* vol. 114, pp. 251-69, Aug 1999.

[66] T. S. Tillman and M. Cascio, "Effects of membrane lipids on ion channel structure and function," *Cell Biochem Biophys,* vol. 38, pp. 161-90, 2003.

[67] N. Gamper and M. S. Shapiro, "Regulation of ion transport proteins by membrane phosphoinositides," *Nat Rev Neurosci,* vol. 8, pp. 921-34, Dec 2007.

[68] T. Rohacs, J. Chen, G. D. Prestwich, and D. E. Logothetis, "Distinct specificities of inwardly rectifying K(+) channels for phosphoinositides," *J Biol Chem,* vol. 274, pp. 36065-72, Dec 17 1999.

[69] P. Aryal, H. Dvir, S. Choe, and P. A. Slesinger, "A discrete alcohol pocket involved in GIRK channel activation," *Nat Neurosci,* vol. 12, pp. 988-95, Aug 2009.

[70] J. P. Ruppersberg, "Intracellular regulation of inward rectifier K+ channels," *Pflugers Arch,* vol. 441, pp. 1-11, Nov 2000.

[71] W. W. L. Cheng, N. D'Avanzo, D. A. Doyle, and C. G. Nichols, "Dual-mode phospholipid regulation of human inward rectifying potassium channels," *Biophys J,* vol. 100, pp. 620-628, Feb 2 2011.

[72] L. H. Xie, S. A. John, B. Ribalet, and J. N. Weiss, "Activation of inwardly rectifying potassium (Kir) channels by phosphatidylinosital-4,5-bisphosphate (PIP2): interaction with other regulatory ligands," *Prog Biophys Mol Biol,* vol. 94, pp. 320-35, Jul 2007.

[73] W. Jin and Z. Lu, "A novel high-affinity inhibitor for inward-rectifier K+ channels," *Biochemistry,* vol. 37, pp. 13291-9, Sep 22 1998.

[74] R. Kanjhan, E. J. Coulson, D. J. Adams, and M. C. Bellingham, "Tertiapin-Q blocks recombinant and native large conductance K+ channels in a use-dependent manner," *J Pharmacol Exp Ther,* vol. 314, pp. 1353-61, Sep 2005.

[75] S. J. Lee, S. Wang, W. Borschel, S. Heyman, J. Gyore, and C. G. Nichols, "Secondary anionic phospholipid binding site and gating mechanism in Kir2.1 inward rectifier channels," *Nat Commun,* vol. 4, p. 2786, 2013.

[76] Z. Su, E. C. Brown, W. Wang, and R. MacKinnon, "Novel cell-free high-throughput screening method for pharmacological tools targeting K+ channels," *Proc Natl Acad Sci U S A,* vol. 113, pp. 5748-53, May 17 2016.

[77] M. R. Whorton and R. MacKinnon, "Crystal structure of the mammalian GIRK2 K+ channel and gating regulation by G proteins, PIP2, and sodium," *Cell,* vol. 147, pp. 199-208, Sep 30 2011.

[78] M. R. Whorton and R. MacKinnon, "X-ray structure of the mammalian GIRK2-betagamma G-protein complex," *Nature,* vol. 498, pp. 190-7, Jun 13 2013.

[79] N. D'Avanzo, W. W. Cheng, D. A. Doyle, and C. G. Nichols, "Direct and specific activation of human inward rectifier K+ channels by membrane phosphatidylinositol 4,5-bisphosphate," *J Biol Chem,* vol. 285, pp. 37129-32, Nov 26 2010.

[80] N. D'Avanzo, S. J. Lee, W. W. Cheng, and C. G. Nichols, "Energetics and location of phosphoinositide binding in human Kir2.1 channels," *J Biol Chem,* vol. 288, pp. 16726-37, Jun 7 2013.

[81] A. Traynor-Kaplan, M. Kruse, E. J. Dickson, G. Dai, O. Vivas, H. Yu, *et al.*, "Fatty-acyl chain profiles of cellular phosphoinositides," *Biochim Biophys Acta,* vol. 1862, pp. 513-522, May 2017.

[82] S. J. Lee, F. Ren, E. M. Zangerl-Plessl, S. Heyman, A. Stary-Weinzinger, P. Yuan, *et al.*, "Structural basis of control of inward rectifier Kir2 channel gating by bulk anionic phospholipids," *J Gen Physiol,* vol. 148, pp. 227-37, Sep 2016.

[83] J. Marcoux, S. C. Wang, A. Politis, E. Reading, J. Ma, P. C. Biggin, *et al.*, "Mass spectrometry reveals synergistic effects of nucleotides, lipids, and drugs binding to a multidrug resistance efflux pump," *Proc Natl Acad Sci U S A,* vol. 110, pp. 9704-9, Jun 11 2013.

[84] G. R. Hilton and J. L. Benesch, "Two decades of studying non-covalent biomolecular assemblies by means of electrospray ionization mass spectrometry," *J R Soc Interface,* vol. 9, pp. 801-16, May 7 2012.

[85] A. Dyachenko, R. Gruber, L. Shimon, A. Horovitz, and M. Sharon, "Allosteric mechanisms can be distinguished using structural mass spectrometry," *Proc Natl Acad Sci U S A,* vol. 110, pp. 7235-9, Apr 30 2013.

[86] D. Cubrilovic, W. Haap, K. Barylyuk, A. Ruf, M. Badertscher, M. Gubler, *et al.*, "Determination of protein-ligand binding constants of a cooperatively regulated tetrameric enzyme using electrospray mass spectrometry," *ACS Chem Biol,* vol. 9, pp. 218-26, Jan 17 2014.

[87] Y. Liu, X. Cong, W. Liu, and A. Laganowsky, "Characterization of Membrane Protein-Lipid Interactions by Mass Spectrometry Ion Mobility Mass Spectrometry," *J Am Soc Mass Spectrom,* vol. 28, pp. 579-586, Apr 2017.

[88] X. Cong, Y. Liu, W. Liu, X. Liang, and A. Laganowsky, "Allosteric modulation of protein-protein interactions by individual lipid binding events," *Nat Commun,* vol. 8, p. 2203, Dec 19 2017.

[89] R. Daneshfar, E. N. Kitova, and J. S. Klassen, "Determination of protein-ligand association thermochemistry using variable-temperature nanoelectrospray mass spectrometry," *J Am Chem Soc,* vol. 126, pp. 4786-7, Apr 21 2004.

[90] K. Gupta, J. A. C. Donlan, J. T. S. Hopper, P. Uzdavinys, M. Landreh, W. B. Struwe, *et al.*, "The role of interfacial lipids in stabilizing membrane protein oligomers," *Nature,* vol. 541, pp. 421-424, Jan 19 2017.

[91] J. W. Patrick, C. D. Boone, W. Liu, G. M. Conover, Y. Liu, X. Cong, *et al.*, "Allostery revealed within lipid binding events to membrane proteins," *Proc Natl Acad Sci U S A,* vol. 115, pp. 2976-2981, Mar 20 2018.

[92] J. R. Bolla, J. B. Sauer, D. Wu, S. Mehmood, T. M. Allison, and C. V. Robinson, "Direct observation of the influence of cardiolipin and antibiotics on lipid II binding to MurJ," *Nat Chem,* vol. 10, pp. 363-371, Mar 2018.

[93] H. Y. Yen, J. T. S. Hopper, I. Liko, T. M. Allison, Y. Zhu, D. Wang, *et al.*, "Ligand binding to a G protein-coupled receptor captured in a mass spectrometer," *Sci Adv,* vol. 3, p. e1701016, Jun 2017.

[94] C. S. Gandhi, T. A. Walton, and D. C. Rees, "OCAM: a new tool for studying the oligomeric diversity of MscL channels," *Protein Sci,* vol. 20, pp. 313-26, Feb 2011.

[95] M. T. Marty, A. J. Baldwin, E. G. Marklund, G. K. Hochberg, J. L. Benesch, and C. V. Robinson, "Bayesian deconvolution of mass and ion mobility spectra: from binary interactions to polydisperse ensembles," *Anal Chem,* vol. 87, pp. 4370-6, Apr 21 2015.

[96] M. L. Poltash, J. W. McCabe, J. W. Patrick, A. Laganowsky, and D. H. Russell, "Development and Evaluation of a Reverse-Entry Ion Source Orbitrap Mass Spectrometer," *J Am Soc Mass Spectrom,* May 23 2018.

[97] S. Mehmood, J. Marcoux, J. T. Hopper, T. M. Allison, I. Liko, A. J. Borysik, *et al.*, "Charge reduction stabilizes intact membrane protein complexes for mass spectrometry," *J Am Chem Soc,* vol. 136, pp. 17010-2, Dec 10 2014.

[98] M. L. Poltash, J. W. McCabe, J. W. Patrick, A. Laganowsky, and D. H. Russell, "Development and Evaluation of a Reverse-Entry Ion Source Orbitrap Mass Spectrometer," *Journal of The American Society for Mass Spectrometry,* 2018/05/23 2018.

[99] M. L. Poltash, J. W. McCabe, M. Shirzadeh, A. Laganowsky, B. H. Clowers, and D. H. Russell, "Fourier Transform-Ion Mobility-Orbitrap Mass Spectrometer: A Next-Generation Instrument for Native Mass Spectrometry," *Anal Chem,* Aug 22 2018.

[100] J. L. Lippens, P. F. Egea, C. Spahr, A. Vaish, J. E. Keener, M. T. Marty, *et al.*, "Rapid LC-MS Method for Accurate Molecular Weight Determination of Membrane and Hydrophobic Proteins," *Anal Chem,* vol. 90, pp. 13616-13623, Nov 20 2018.

[101] J. W. Sherman F Fau - Stewart, S. Stewart Jw Fau - Tsunasawa, and S. Tsunasawa, "Methionine or not methionine at the beginning of a protein."

[102] P. T. Wingfield, "N-Terminal Methionine Processing," *Curr Protoc Protein Sci,* vol. 88, pp. 6 14 1-6 14 3, Apr 3 2017.

[103] W. Jin and Z. Lu, "Synthesis of a stable form of tertiapin: a high-affinity inhibitor for inward-rectifier K+ channels," *Biochemistry,* vol. 38, pp. 14286-93, Oct 26 1999.

[104] A. Laganowsky, E. Reading, T. M. Allison, M. B. Ulmschneider, M. T. Degiacomi, A. J. Baldwin, *et al.*, "Membrane proteins bind lipids selectively to modulate their structure and function," *Nature,* vol. 510, pp. 172-175, Jun 05 2014.

[105] I. S. Chen, M. Tateyama, Y. Fukata, M. Uesugi, and Y. Kubo, "Ivermectin activates GIRK channels in a PIP2 -dependent, Gbetagamma -independent manner and an amino acid residue at the slide helix governs the activation," *J Physiol,* vol. 595, pp. 5895-5912, Sep 1 2017.

[106] R. A. Copeland, D. L. Pompliano, and T. D. Meek, "Drug-target residence time and its implications for lead optimization," *Nat Rev Drug Discov,* vol. 5, pp. 730-9, Sep 2006.

[107] H. Yin and A. D. Flynn, "Drugging Membrane Protein Interactions," *Annu Rev Biomed Eng,* vol. 18, pp. 51-76, Jul 11 2016.

[108] S. K. Adney, J. Ha, X. Y. Meng, T. Kawano, and D. E. Logothetis, "A Critical Gating Switch at a Modulatory Site in Neuronal Kir3 Channels," *J Neurosci,* vol. 35, pp. 14397-405, Oct 21 2015.

[109] J. Mao, X. Wang, F. Chen, R. Wang, A. Rojas, Y. Shi, *et al.*, "Molecular basis for the inhibition of G protein-coupled inward rectifier K(+) channels by protein kinase C," *Proc Natl Acad Sci U S A,* vol. 101, pp. 1087-92, Jan 27 2004.

[110] H. J. Chung, X. Qian, M. Ehlers, Y. N. Jan, and L. Y. Jan, "Neuronal activity regulates phosphorylation-dependent surface delivery of G protein-activated inwardly rectifying potassium channels," *Proc Natl Acad Sci U S A,* vol. 106, pp. 629-34, Jan 13 2009.

[111] T. Harayama and H. Riezman, "Understanding the diversity of membrane lipid composition," *Nat Rev Mol Cell Biol,* vol. 19, pp. 281-296, May 2018.

[112] J. Monod, J. Wyman, and J. P. Changeux, "On the Nature of Allosteric Transitions: A Plausible Model," *J Mol Biol,* vol. 12, pp. 88-118, May 1965.

[113] H. N. Motlagh, J. O. Wrabl, J. Li, and V. J. Hilser, "The ensemble nature of allostery," *Nature,* vol. 508, pp. 331-9, Apr 17 2014.

[114] J. Liu and R. Nussinov, "Allostery: An Overview of Its History, Concepts, Methods, and Applications," *PLoS Comput Biol*, vol. 12, p. e1004966, Jun 2016.

[115] H. Zhang, C. He, X. Yan, T. Mirshahi, and D. E. Logothetis, "Activation of inwardly rectifying K+ channels by distinct PtdIns(4,5)P2 interactions," *Nat Cell Biol*, vol. 1, pp. 183-8, Jul 1999.

[116] H. Y. Yen, K. K. Hoi, I. Liko, G. Hedger, M. R. Horrell, W. Song, *et al.*, "PtdIns(4,5)P2 stabilizes active states of GPCRs and enhances selectivity of G-protein coupling," *Nature*, vol. 559, pp. 423-427, Jul 2018.

APPENDIX A

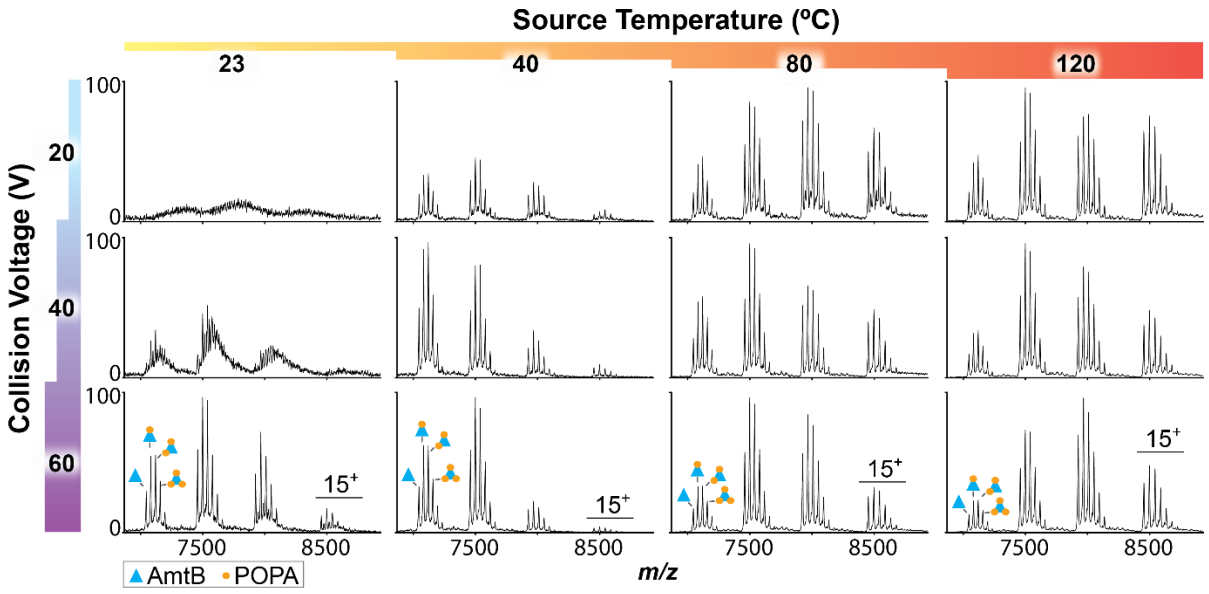

Figure 1. Representative mass spectra of AmtB bound to 1-palmitoyl-2-oleoyl phosphatidic acid (POPA) recorded at different source temperatures and collision voltages. The mass spectrum acquired at ambient source temperature (23 °C) produced an unresolved spectrum at the two lowest collision voltage settings. Given the configuration of the Synapt G1 instrument [40], these results demonstrate the necessity of "in-source" activation prior to entrance into the quadrupole such that resolved ions can be isolated. Increasing source temperature activates ions comparably to increased collision voltage settings at ambient source temperature.

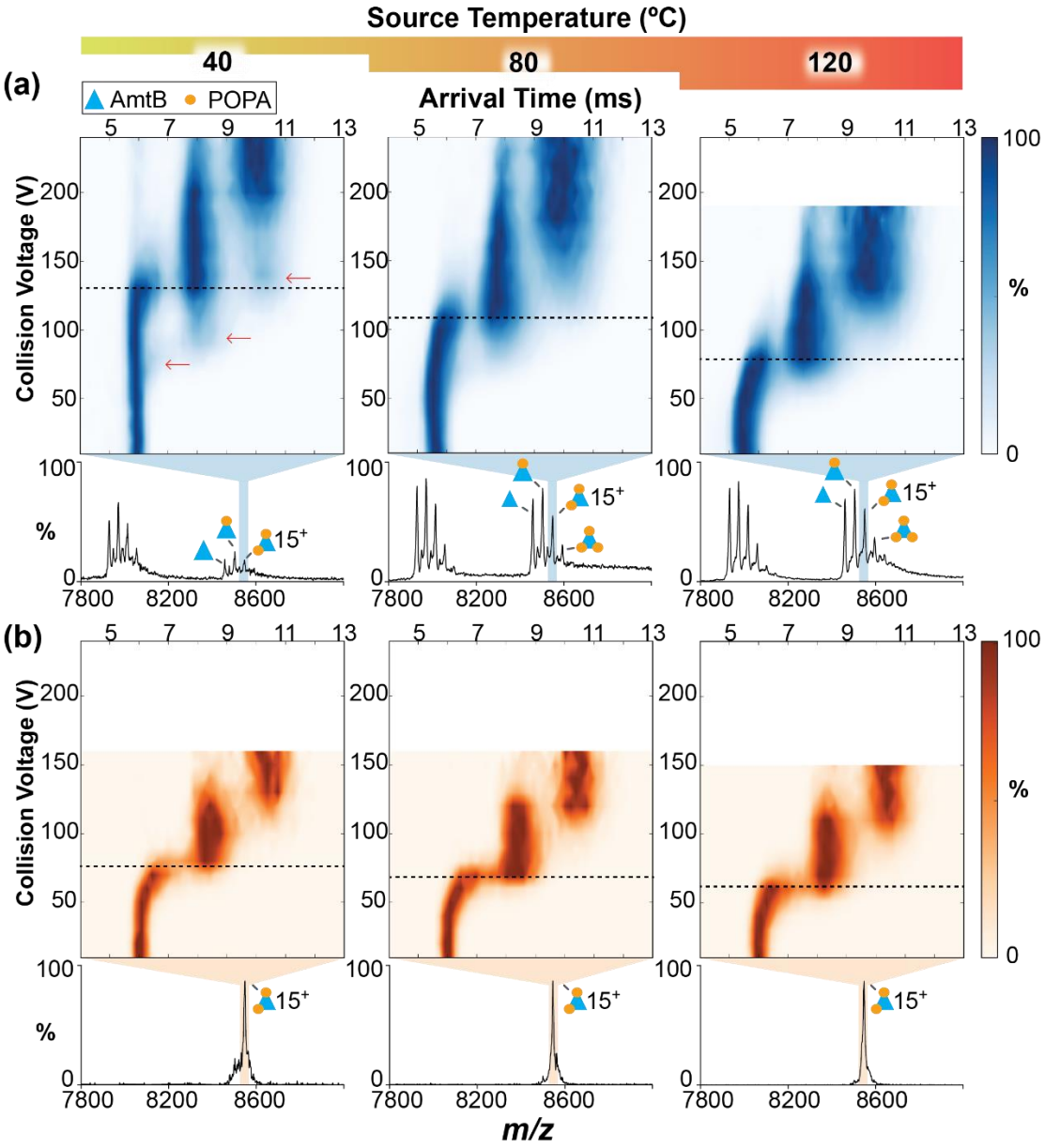

Figure 2. Collision induced unfolding (CIU) profile of the 15^{+} charge state of AmtB bound to two 1-palmitoyl-2-oleoyl phosphatidic acid (POPA). Shown are CIU profiles acquired using either (a) IM-MS or (b) MS-IM-MS with source temperature set to 40, 80 or 120 ºC. CIU profiles were generated using the software program, Pulsar [35]. Representative mass spectrum recorded at a collision voltage of 20 V is shown with their respective CIU profiles recorded at different source temperatures. The first transition from a native-like to a partially unfolding intermediate, calculated by Pulsar, is shown as a dashed line. The faint overlay of MS-IM-MS CIU profile in the IM-MS CIU profile (a, left panel) is indicated by red arrows.

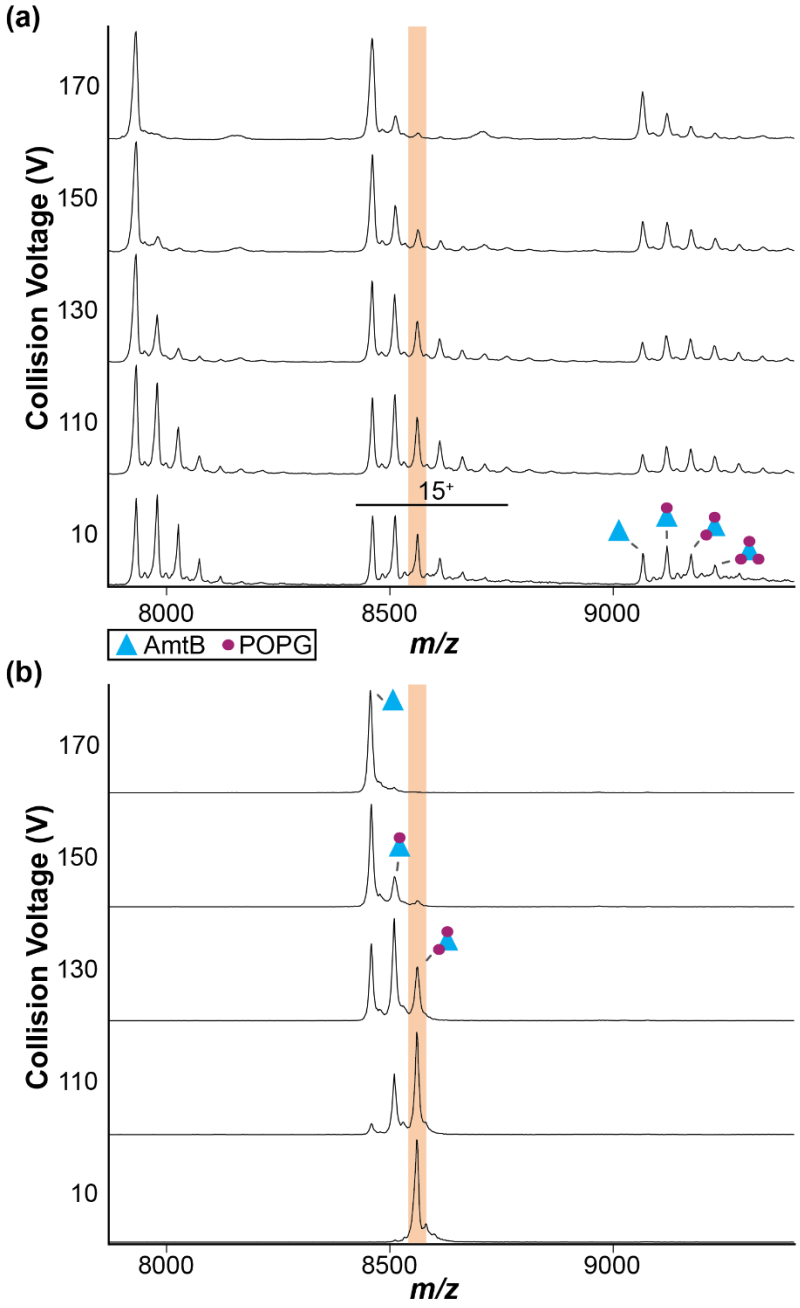

Figure 3. MS and MS-IM-MS of AmtB in complex with 1-palmitoyl-2-oleoyl phosphotidylglycerol (POPG) recorded at different collision voltages and source temperature of 120 ºC. (a) Representative mass spectrum of AmtB bound to POPG under native-like conditions. (b) Isolation of the 15^{+} charge state of AmtB$(POPG)_2$ prior to activation in the trap (bottom panel). Upon activation in the trap, bound POPG molecules are ejected as a neutral species with increasing trap collision voltage.

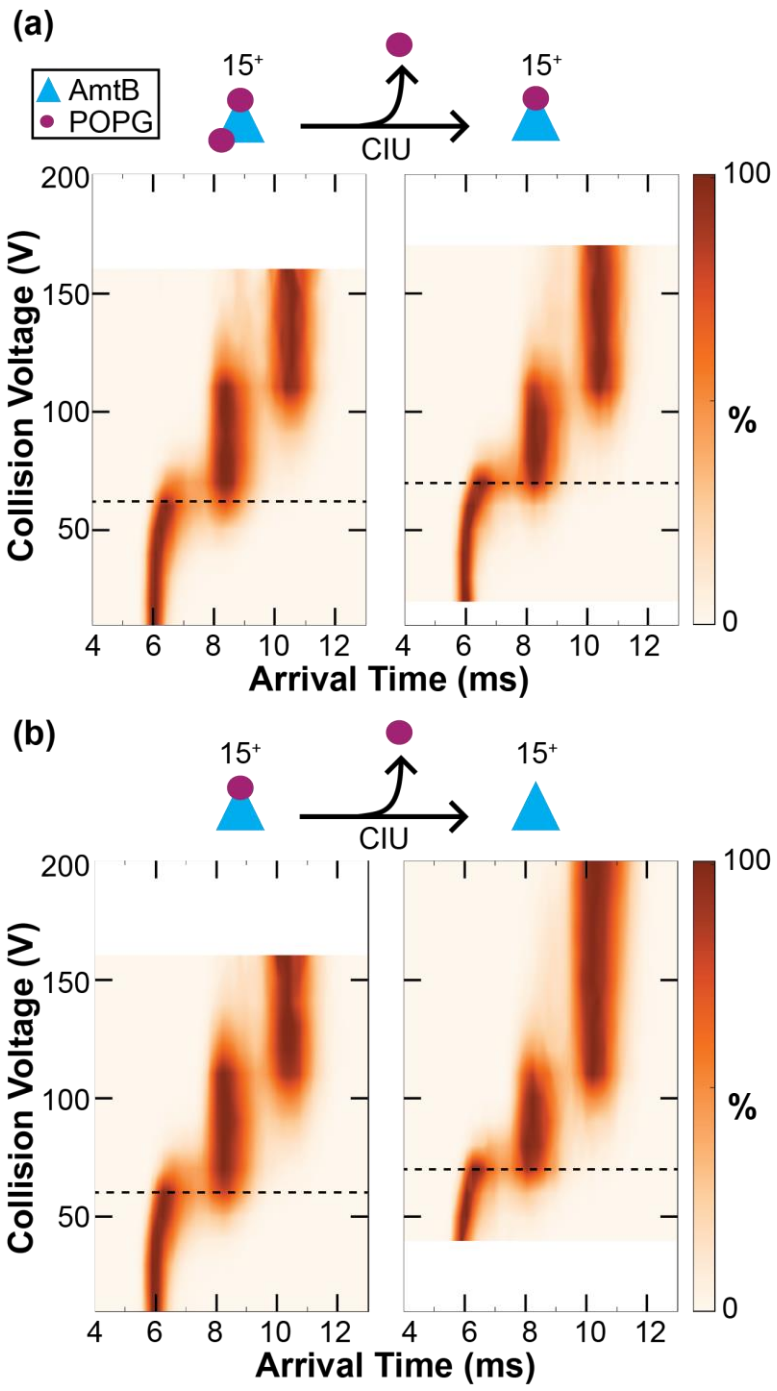

Figure 4. MS-IM-MS CIU profiles of AmtB bound to (a) two or (b) one POPG molecule(s). MS-IM-MS data recorded at a source temperature of 120 ºC. The CIU profile for the product AmtB species minus an ejected lipid is shown on the right. The first transition lines are shown as described in Figure 2.

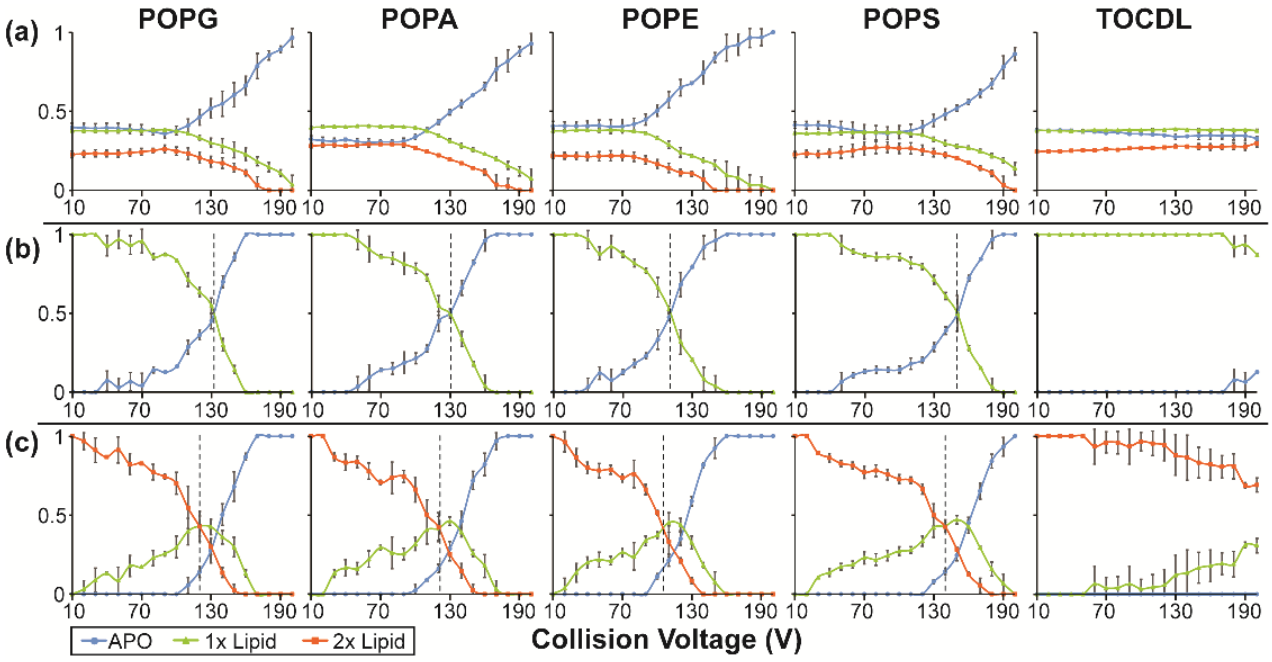

Figure 5. Mole fraction of AmtB lipid species across CIU profiles for (a) IM-MS and MS-IM-MS of AmtB bound to (b) one and (c) two lipid(s). Data was recorded at a source temperature of 120 °C. Dashed lines indicate the estimated collision voltage at which half of the bound lipid has been ejected. Phosphatidylserine (POPS), phosphatidylethanolamine (POPE), and tetra oleoyl (18:1) cardiolipin (TOCDL). Reported are average and standard deviation (*n*=3).

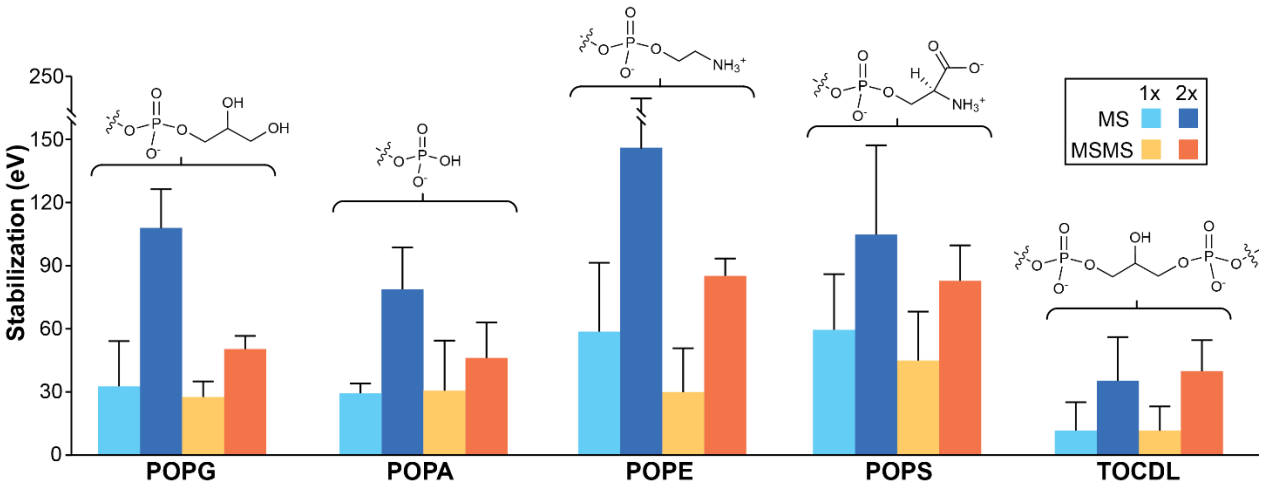

Figure 6. Stabilization of AmtB bound to lipid determined from IM-MS and MS-IM-MS. The head group structure of each lipid is shown. Stabilization was calculated by comparing the transitions in CIU profiles for *apo* and lipid-bound states in units of electron volts using calculation methods described literature [27, 35]. Reported are the average and standard deviation (n=3).

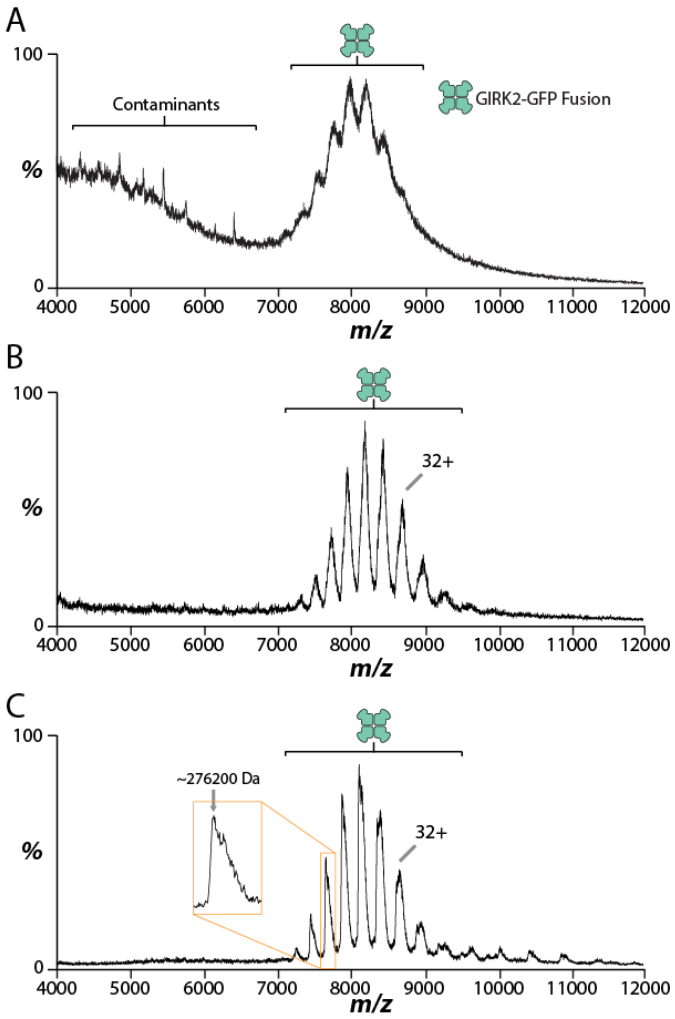

Figure 7. Representative mass spectra of the GIRK2-GFP fusion protein showing the result of detergent screening performed to optimize sample quality for the GIRK2-GFP fusion protein. (A), Initial preparation of GIRK2 extracted in 3% DDM and analyzed in MS buffer containing 0.05% DDM, in a similar fashion to the established protocol for structural studies [78] but without performing size-exclusion chromatography (SEC). The mass of the tetrameric complex cannot be ascertained due to heterogeneous adduct species causing the significant peak broadening. Some contaminant proteins that were co-purified were visible on the left side of the spectrum. (B) GIRK2-GFP purified in 4% NG (n-Nonyl-β-d-glucoside, Anatrace), followed by SEC and MS analysis in buffers containing 0.05% DDM. While still difficult to accurately determine, the mass of the complex is much closer to the calculated average as bound adducts were reduced significantly. (C) GIRK2-GFP purified in 4% DDM, followed by buffer A wash supplemented with 2% NG, then analyzed in MS buffer containing 0.05% DDM. The combinatorial effect of both DDM and NG washes allowed sufficient removal of adducts such that the apo-GIRK2-GFP fusion protein is revealed at roughly 276.2 kDa.

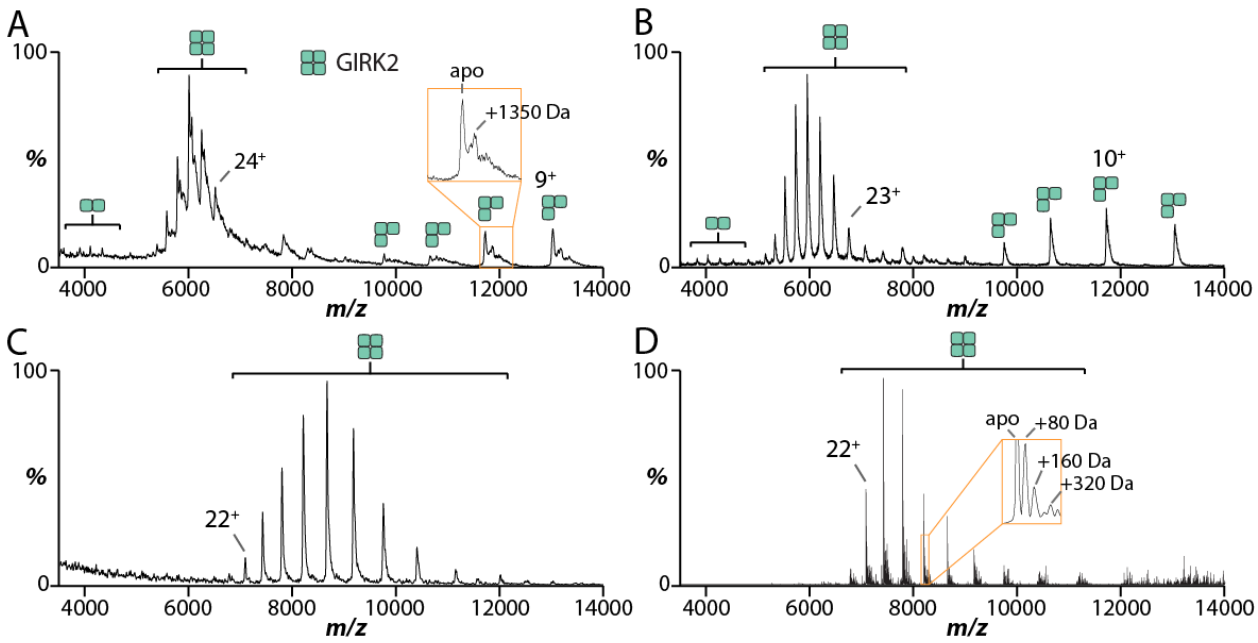

Figure 8. Optimization of mouse GIRK2 for native mass spectrometry studies. (A) Initial preparation of GIRK2 in dodecylmaltoside (DDM) following established protocols for structural studies [77]. The mass spectrum was recorded using maximum energy settings to reveal 1,350 Da adducts bound to GIRK2. (B) Mass spectrum of GIRK2 in DDM after DHPC treatment, which reveals a well resolved mass spectrum with the lipid adducts removed. DHPC treated GIRK2 in the charge-reducing detergent, $C_{10}E_5$ acquired under minimal energy regimes on a (C) Waters Synapt G1 and (D) Thermo Exactive plus EMR modified with a rear-entry source [98]. The mass spectra resolves small molecule adducts bound to the tetrameric complex.

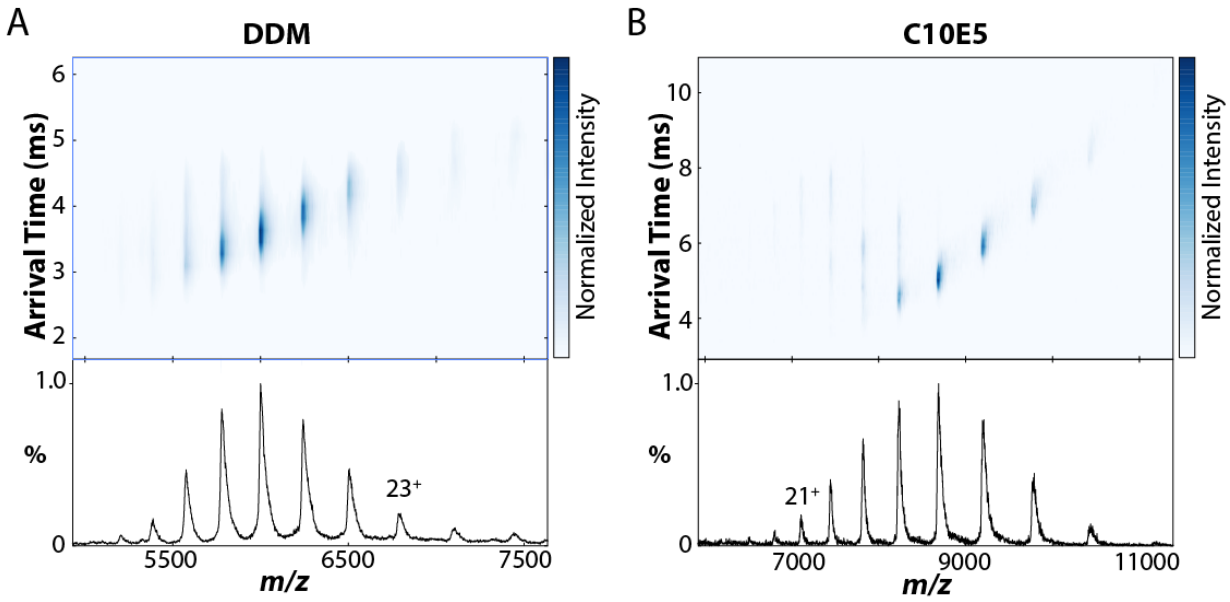

Figure 9. Representative ion mobility mass spectra of GIRK2 tetramer (~156.2 kDa). GIRK2 in MS buffer containing 2x critical micelle concentration (CMC) of (A) DDM or (B) $C_{10}E_5$. The average charge state of GIRK2 in DDM buffer is about 26^+ whereas in $C_{10}E_5$ the average is reduced to about 18^+. Charge reduction afforded additional stability for the GIRK2 complex in the gas-phase, where more than half of the charge states' arrival-times fall on a trend-line that is typically associated with "native-like" protein complexes.

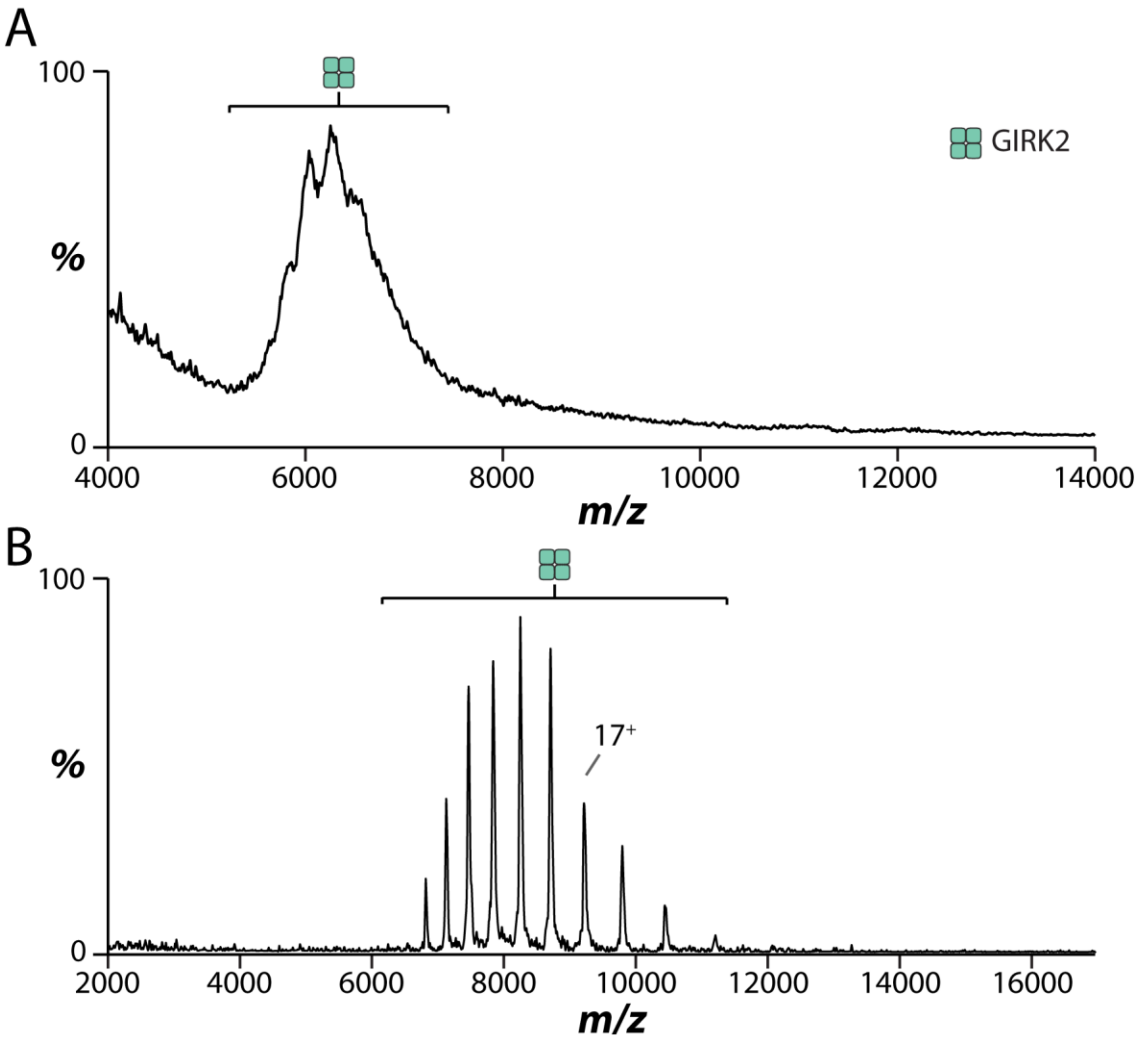

Figure 10. Optimization of sample purification is required to obtain a resolved native mass spectrum. A) Native mass spectrum of GIRK2 purified following previously established methods [77] in DDM collected at the same instrument conditions as in Fig 7C yields a hump with a unresolved mass spectrum. B) Optimized sample in $C_{10}E_5$ after a DHPC treatment as described in methods. The activation energies were 120 V and 80 V for the trap and transfer cell, respectively. No dissociated monomers or stripped oligomers are observed under these experimental conditions for GIRK2 liberated from $C_{10}E_5$.

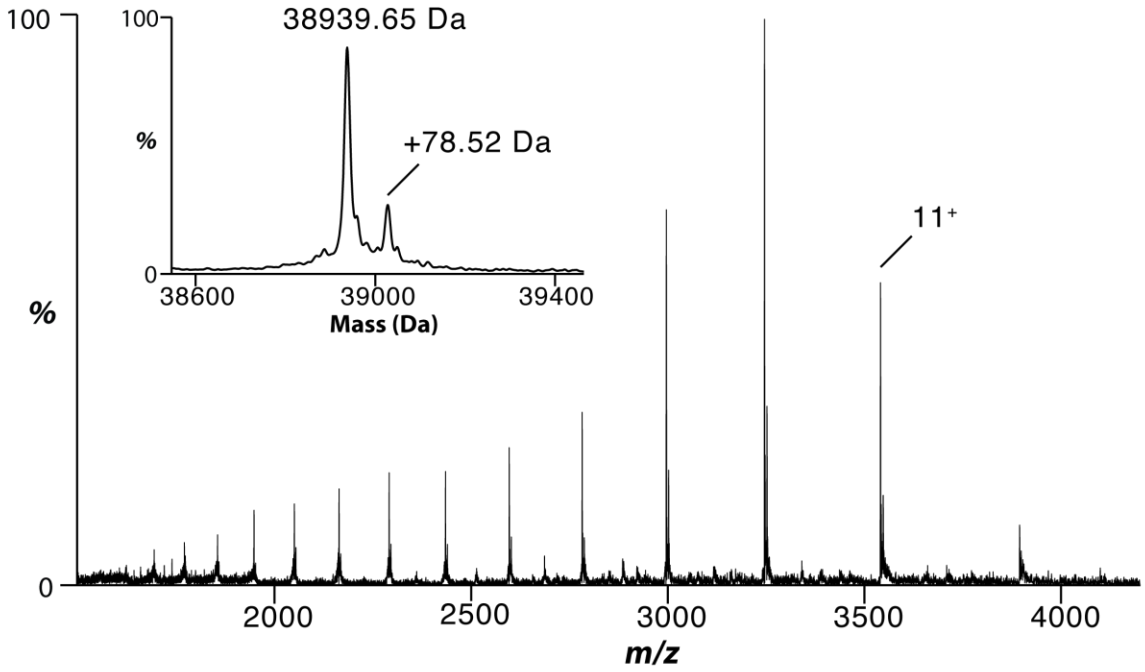

Species	Calculated (Da)	Observed (Da)	Δ Mass (Da)
GIRK2	38941.85*	38939.65 ± 0.82	2.20
Phosphorylation	78.97	78.52 ± 0.82	0.45

Figure 11. Mass spectrum of intact and denatured GIRK2. Inset shows zero-charge mass spectrum with labeled mass species. The table shows the summary of the mass species. *Monomer mass was calculated with the initiating methionine removed. Roughly 19% of signal intensity is attributed to the phosphorylated species.

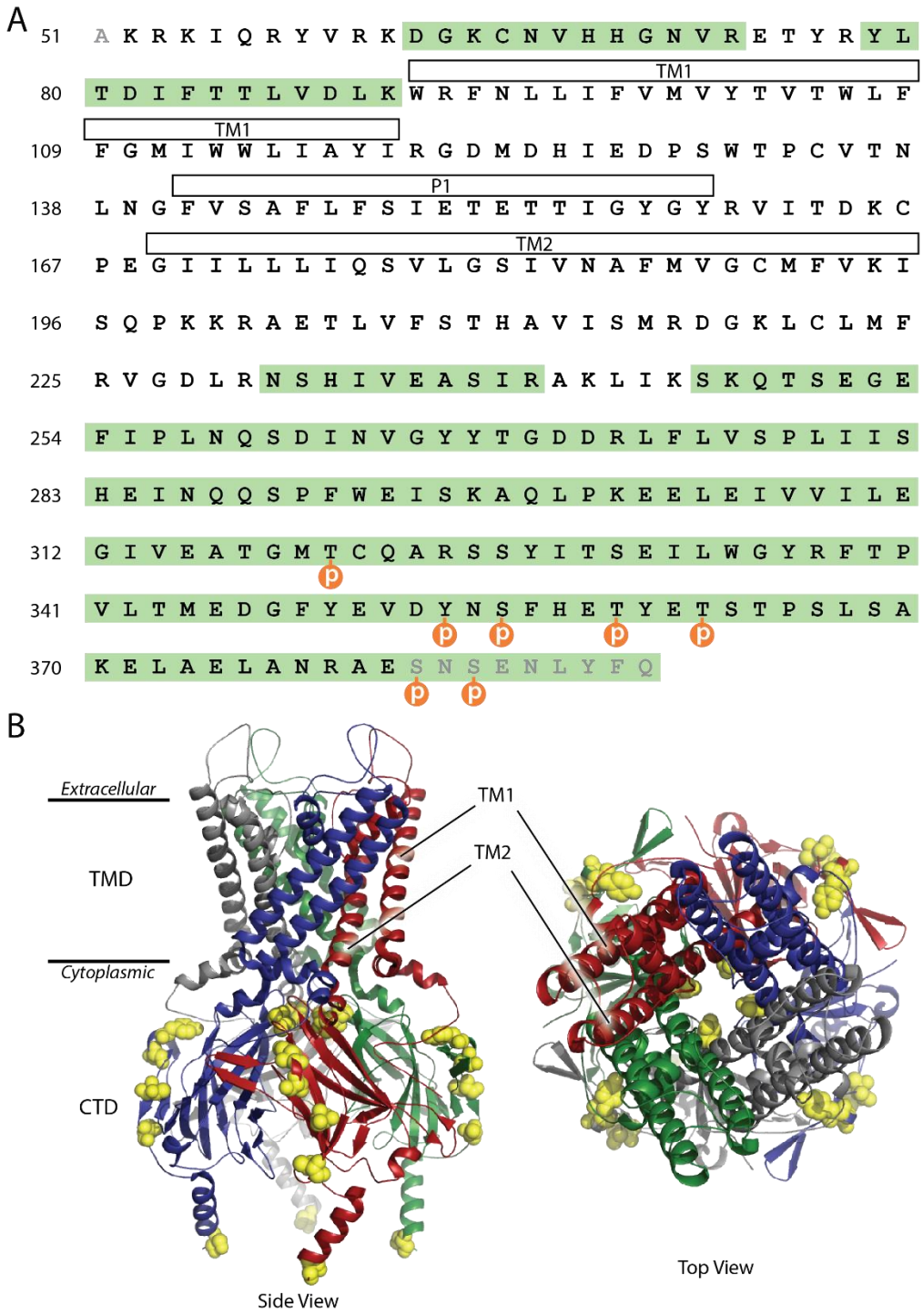

Figure 12. Bottom-up MS analysis of GIRK2 tryptic peptides. A) Sequence coverage (53%) is shown in green and identified phosphorylation sites labeled with an orange circle. Non GIRK2 residues from the expression construct are shown in grey colored font. B) Structural of GIRK2 (PDB 3SYA) with identified phosphorylation sites shown as yellow spheres.

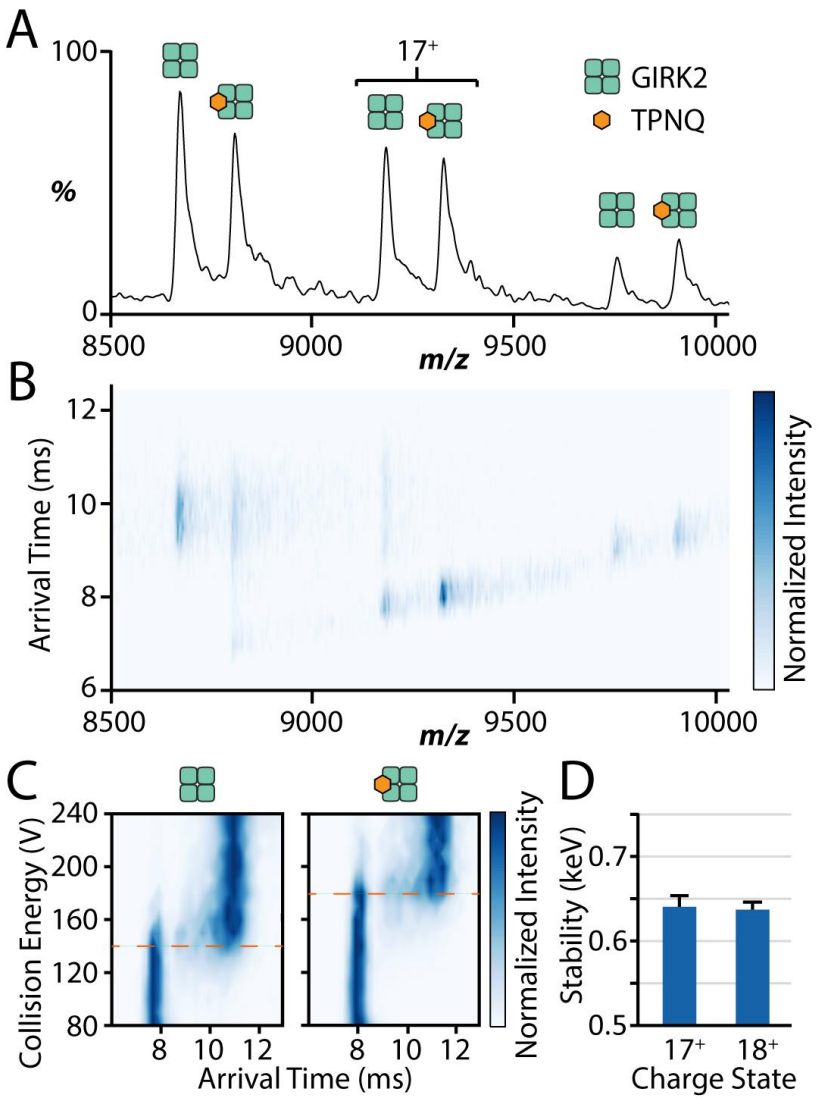

Figure 13. Mass spectrometry captures honey bee toxin, Tertiapin Q (TPNQ) binding and stabilization of GIRK2. (A) Mixture of GIRK2 and six molar equivalents of TPNQ in $C_{10}E_5$. One TPNQ binding event is observed in the mass spectrum. (B) Ion mobility mass spectrum indicates the 17^+ charge state stabilizes the native-like state of the channel when bound to TPNQ. (C) Collision induced unfolding (CIU) plots for the 17^+ charge state (left) apo and (right) TPNQ bound GIRK2. (D) Stabilization calculated from parameters defined by fitting GIRK2 (17^+ and 18^+) bound to TPNQ using the software program, PULSAR [27, 35] Reported are average and standard deviation from repeated measurements (n = 3) in kiloelectron volts (keV).

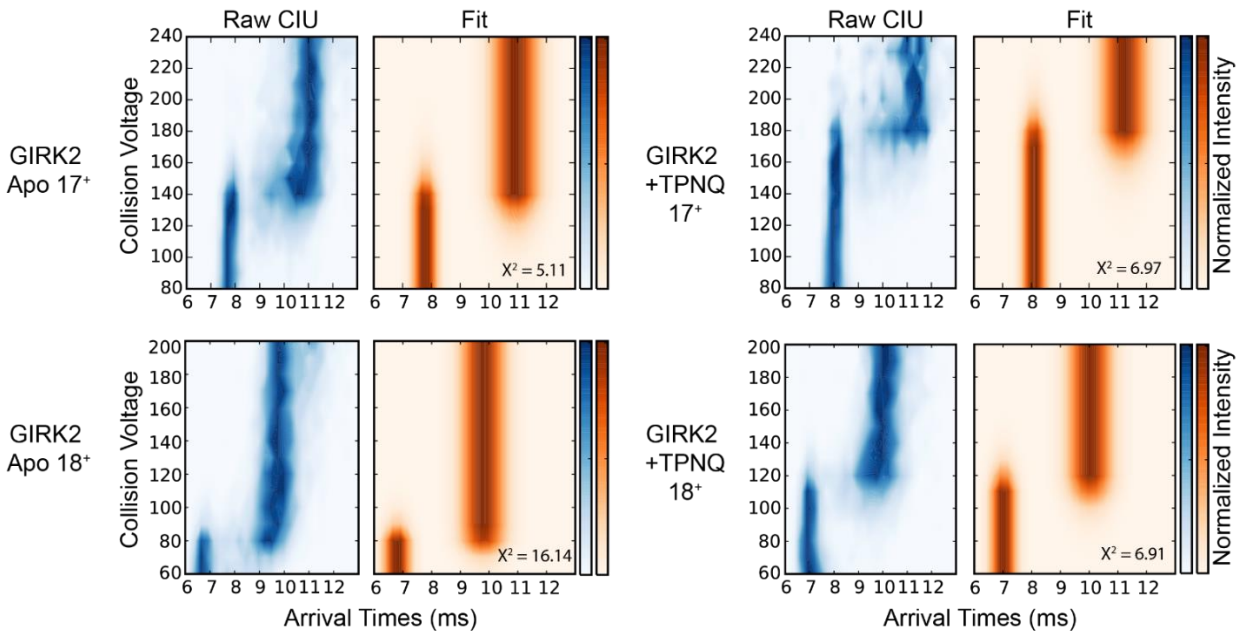

Figure 14. CIU unfolding profiles for 17^{+} and 18^{+} charge states of apo and TPNQ bound GIRK2. The blue plots represent experimental data and orange plots are fits to the experimental data using the software program, PULSAR [35]. Reported in the fitted models is the chi-square fitting statistic from PULSAR. TPNQ binding to GIRK2 significantly stabilizes the channel as evident by large shift in the transition from native-like to a partially unfolded state.

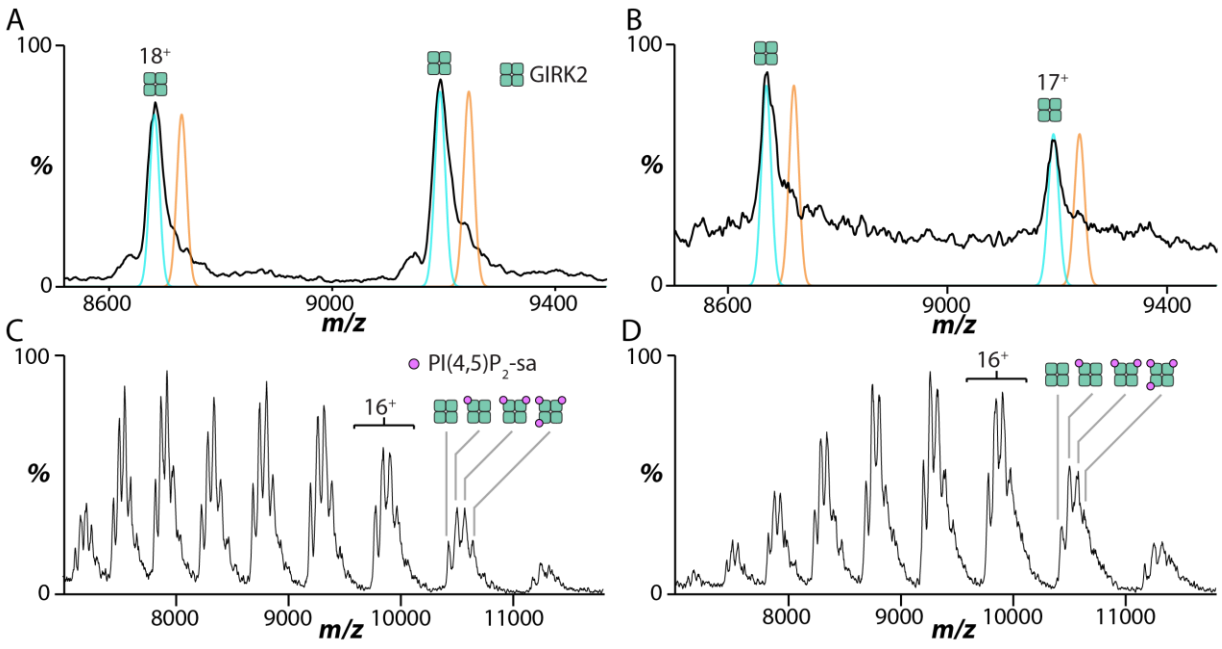

Figure 15. Native mass spectra of GIRK2 doped with ivermectin and/or PI(4,5)P. (A) Representative mass spectrum of GIRK2 showing the 17^+ and 18^+ charge states. Blue lines show the estimated resolution achieved on the GIRK2 complex, and orange lines show hypothetical ivermectin binding events at the same resolving power. (B) Representative mass spectrum showing 17^+ and 18^+ charge state for GIRK2 in the presence of 300 μM ivermectin which is solubilized in MS buffer containing 5% ethanol and 3% DMSO. No binding of ivermectin was observed at the calculated *m/z* values for either wild-type or $GIRK2^{R201A}$ (data not shown for $GIRK2^{R201A}$ or concentrations below 300 μM) (C) Mass spectrum of mixture containing 500 nM GIRK2 and 3 μM $PI(4,5)P_2$-sa, the most abundance form of $PI(4,5)P_2$ in mammalian cells [81]. (D) Native mass spectrum for a mixture of 500 nM GIRK2, 3μM $PI(4,5)P_2$-sa and 50 μM ivermectin. No changes to the lipid binding pattern is observed in the presence of ivermectin, but there is a shift in the overall charge-state distribution.

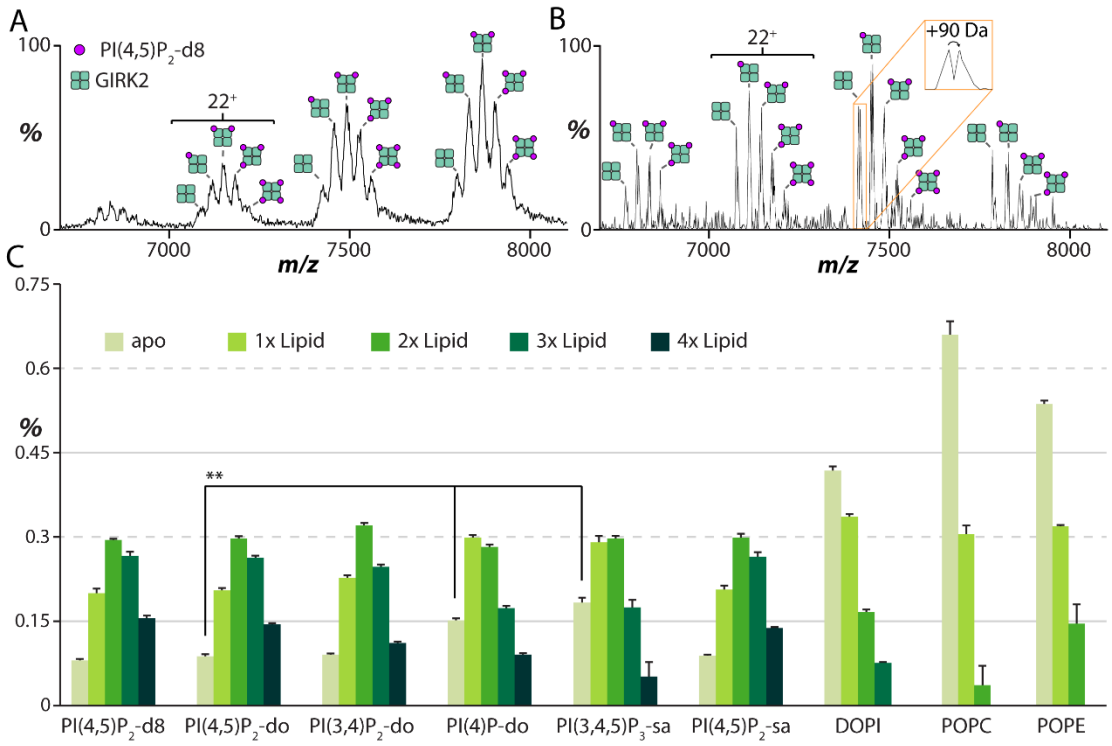

Figure 16. Selective binding of PIPs and phospholipids to GIRK2. Representative mass spectra of a mixture of 0.5 µM GIRK2 and 3 µM PI(4,5)P_2-d8 acquired on the (A) Synapt G1 and (B) Exactive Plus EMR. Up to four lipid binding events are observed in the mass spectra, and higher resolution achieved by the EMR enabling small molecule adducts to be resolved. (C) Plot of mole fraction data obtained from deconvoluting mass spectra for various lipids mixed with GIRK2 at a molar ratio of 6:1, respectively. GIRK2 has much higher affinity for PIPs over other phospholipids. Reported is the average and s.e.m. (n = 3). Student's t-test (two-tailed) was used for statistical analysis (**P<0.01) with the apo molar fraction being used for comparison. Lipid abbreviations are provided in Table S2.

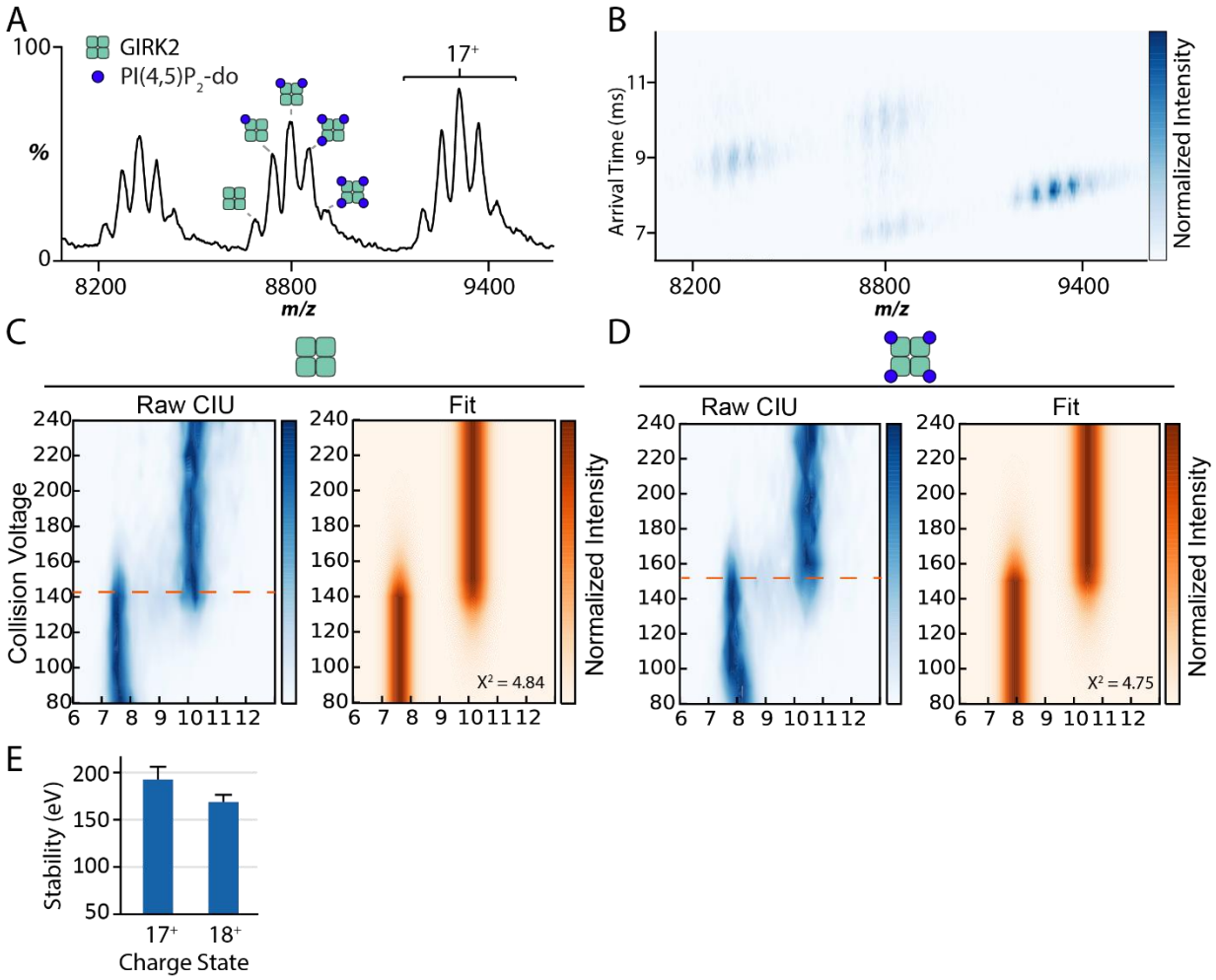

Figure 17. Collision inducing unfolding plots for apo and PIP2 bound GIRK2. (A) and (B) shows the mass and ion-mobility spectrum for GIRK2 bound to PI(4,5)P2-do, respectively. (C) and (D) shows the CIU profiles and the fitted model for unfolding of apo GIRK2 and GIRK2 bound to four PI(4,5)P2-do molecules, respectively. (E) Stabilization calculated from parameters defined by fitting GIRK 17^{+} and 18^{+} bound to four PI(4,5)P2-do molecules. Reported are average and standard deviation from repeated measurements (n=3) in electron volts (eV).

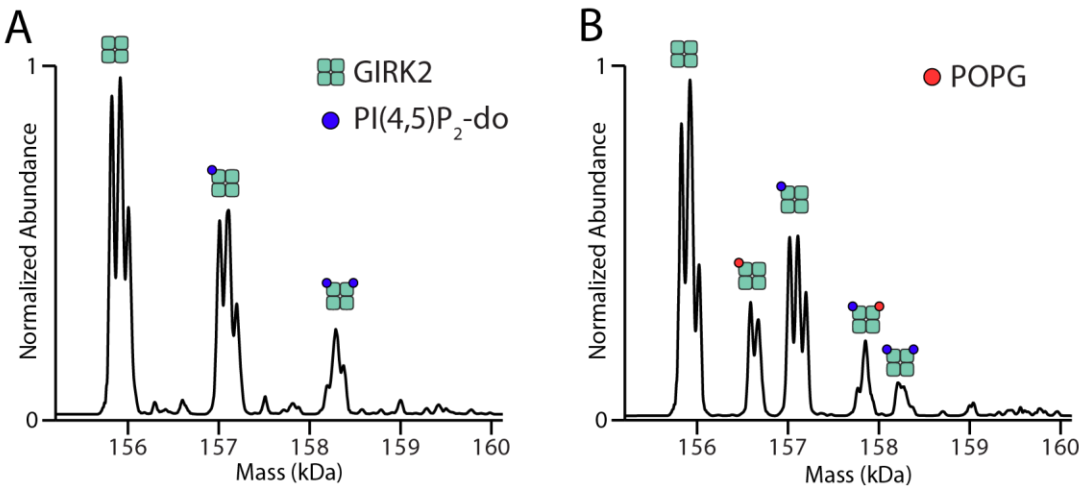

Figure 18. Deconvolution of high-resolution native mass spectra of GIRK2 bound to different lipids. (A) GIRK2 incubated with four molar equivalents of PI(4,5)P_2-do. (B) GIRK2 incubated with a equimolar mixture of POPG and PI(4,5)P_2-do. For the mixture, no change in binding of PI(4,5)P_2-do is observed that would indicate competition or positive allosteric modulation.

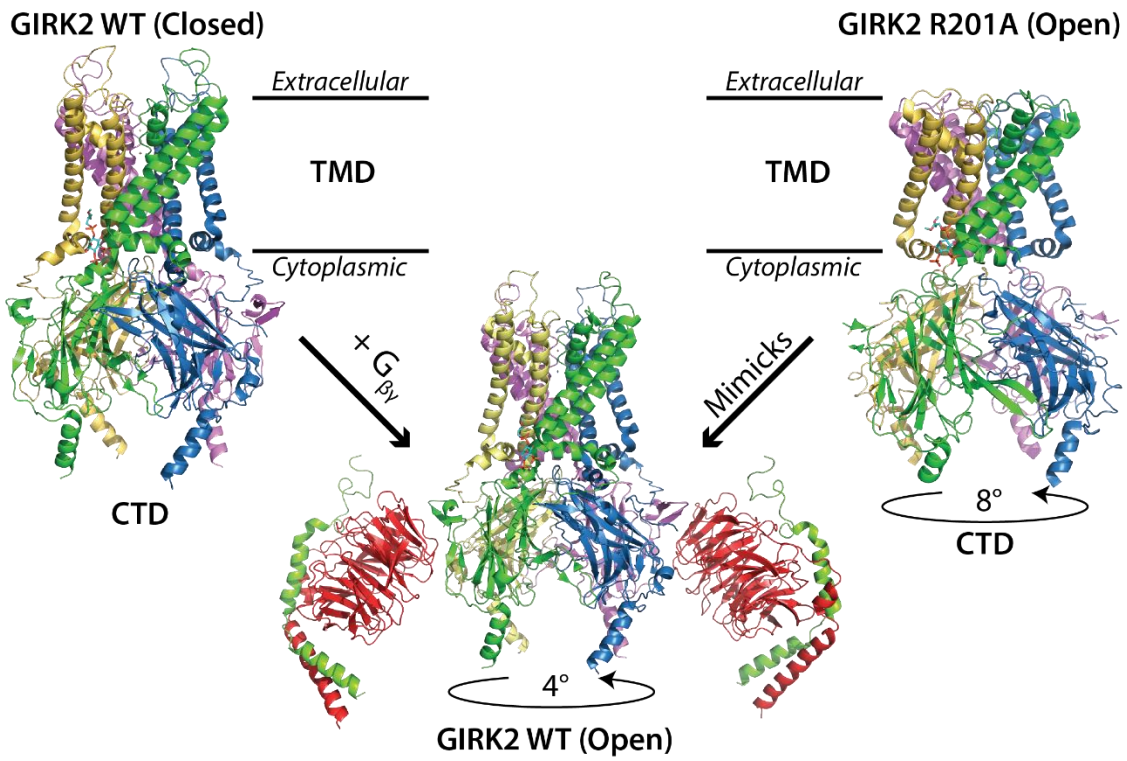

Figure 19. Stuctures of wild-type GIRK2 (PDB 3SYA), R201A (3SYQ) and comparison between the cytoplasmic domain (CTD) rotation as a result of the mutation. Center bottom shows the Gβγ bound form of wild-type GIRK2 (PDB 4KFM). The rotation of the GIRK2 R201A's CTD mimics the structure of the "open" form of the WT as a result of Gβγ binding.

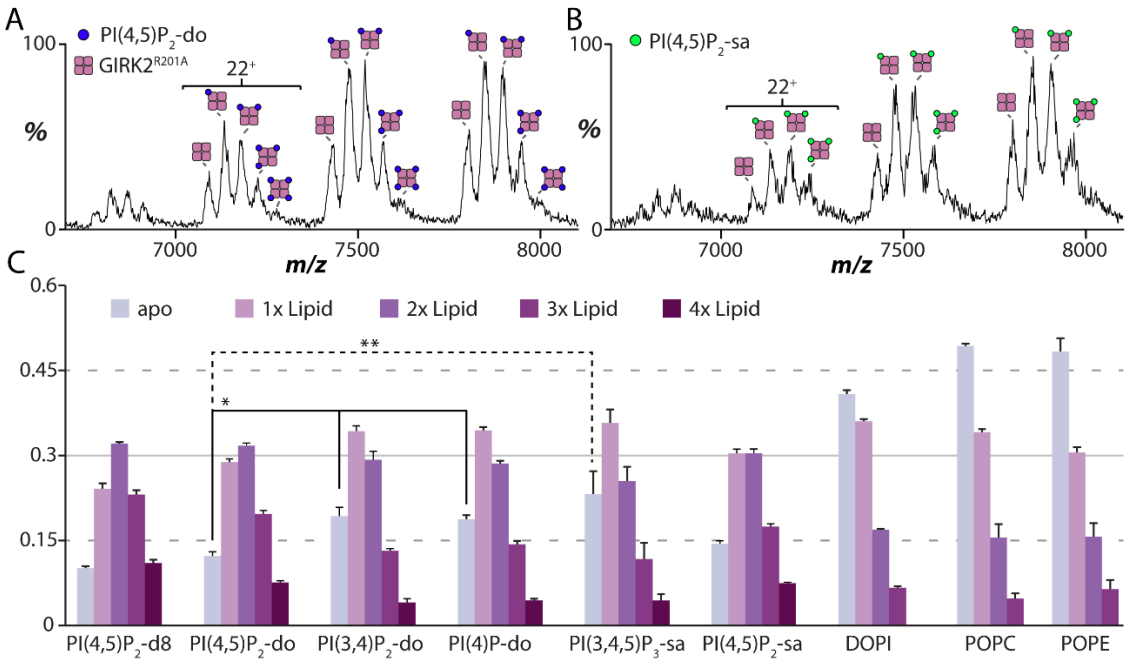

Figure 20. Mass spectrometry reveals a change in the selectivity of GIRK^{R201A}, a channel with CTD rotation that has been proposed to mimic the $G_{\beta\gamma}$-activated state, towards PIPs and phospholipids. Representative mass spectra of GIRK2^{R201A} mixed with six equivalents of (A) PI(4,5)P_2-do and (B) PI(4,5)P_2-sa. (C) Mole fraction derived from mass spectrometry data for GIRK2 mixed with different lipids at six-fold molar excess. Reported is the average and s.e.m. (*n* = 3). Student's *t*-test (two-tailed) was used for statistical analysis (**P*<0.03) as described in Fig 16.

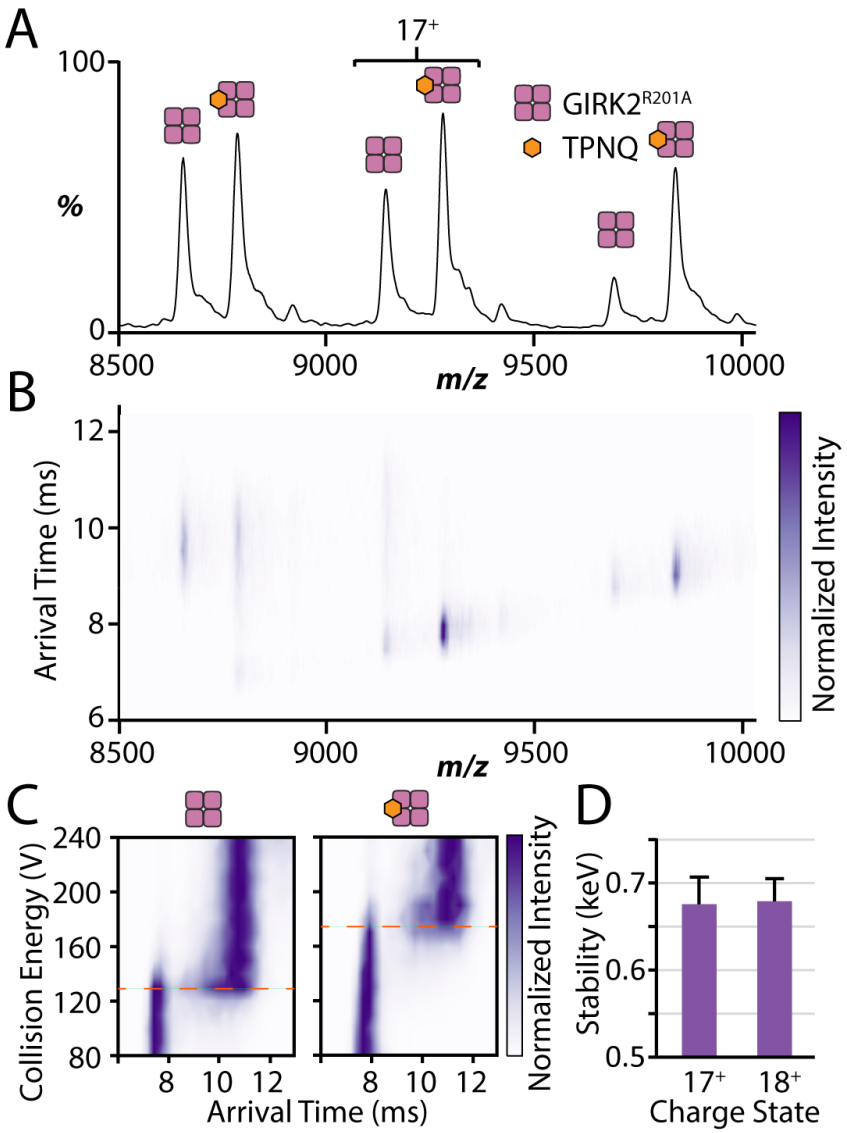

Figure 21. GIRK2^{R201A} mixed with TPNQ reveals the bound toxin significantly stabilizes the channel. (A) Native mass spectrum of GIRK2 mixed with 5 μM TPNQ. (B) Ion mobility mass spectrum showing the arrival times for 16^+, 17^+ and 18^+ charge states. (C) CIU profiles for the 17^+ charge state apo and TPNQ bound GIRK2^{R201A}, orange dotted line indicates the calculated transition voltage from PULSAR [35]. (D) Stabilization calculated from parameters defined by fitting GIRK2 (17^+ and 18^+) bound to TPNQ. Reported are average and standard deviation from repeated measurements (n=3) in electron volts (eV). Stabilization of the mutant channel by TPNQ is statistically similar to wild-type channel.

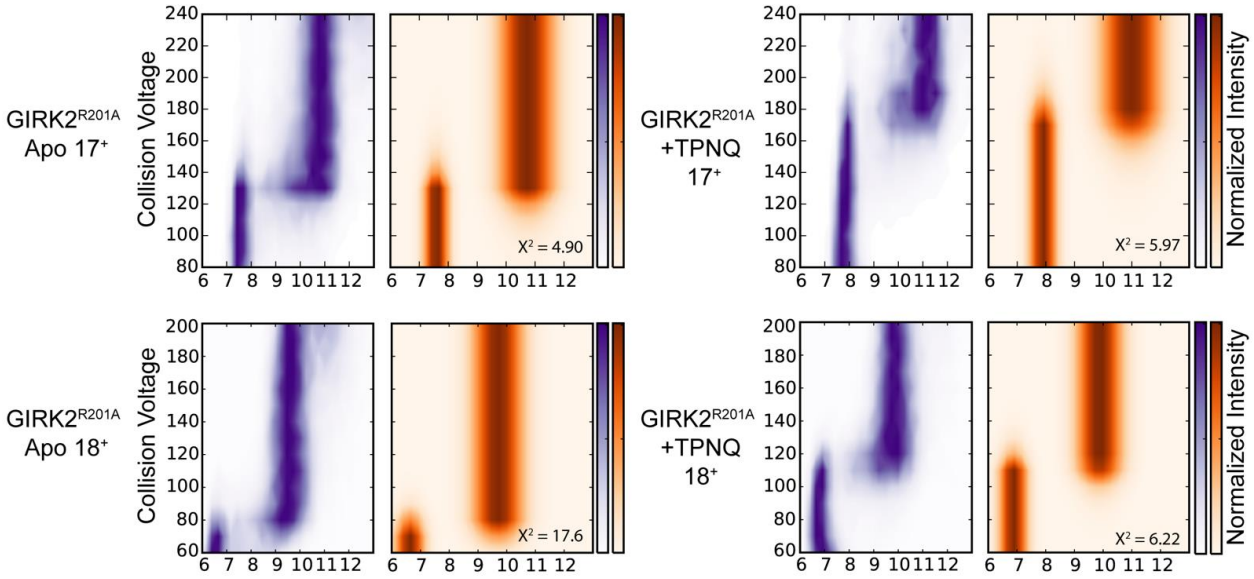

Figure 22. CIU unfolding profiles for both 17^{+} and 18^{+} charge states of apo and TPNQ bound $GIRK2^{R201A}$. Shown as described in Figure 14.

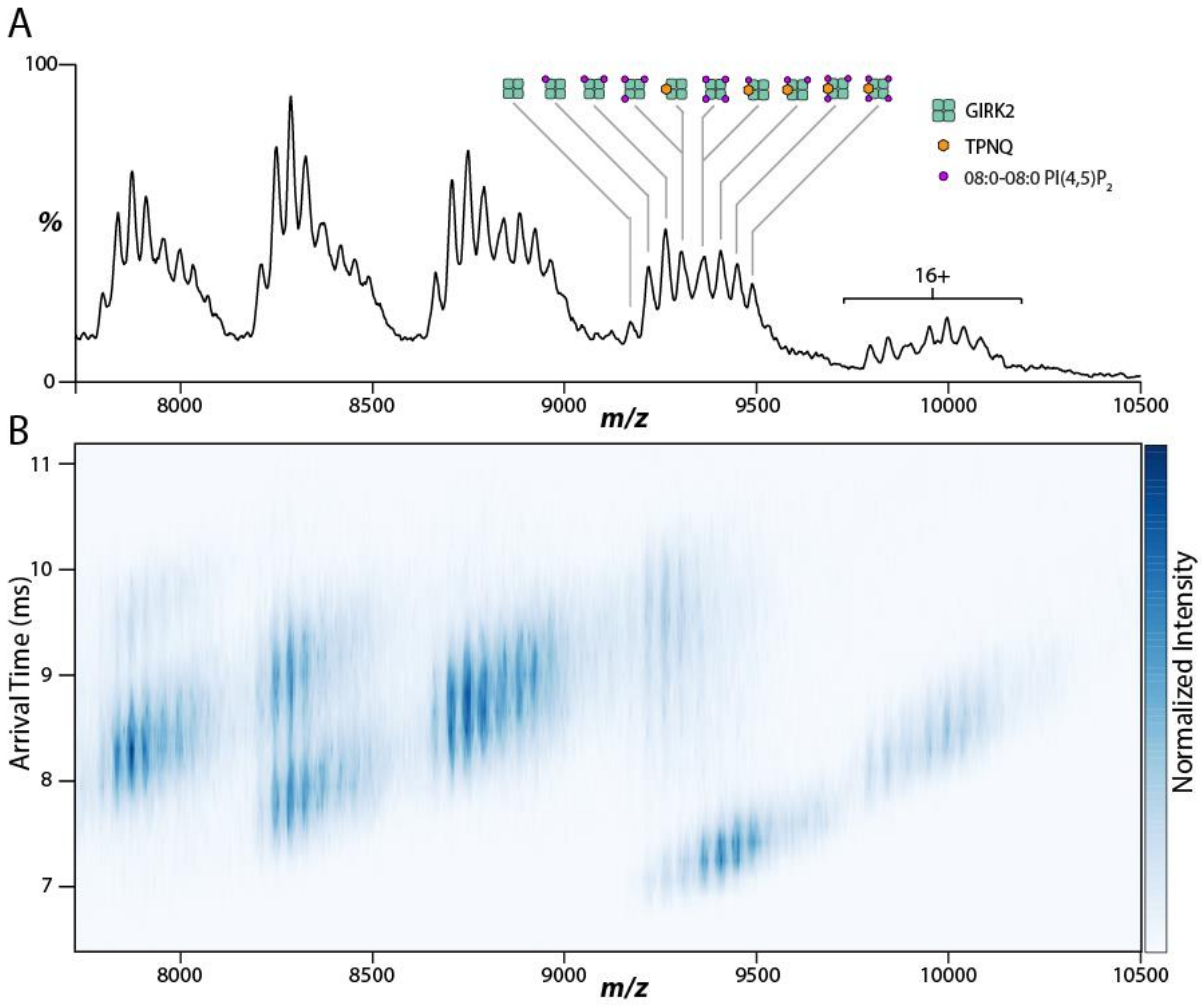

Figure 23. Representative mass and ion mobility spectrum of GIRK2 in the presence of both TPNQ and PI(4,5)P2-d8. (A) Mass spectra of the complex showing mass species for the GIRK2 complex and its various ligand-bound arrangements. Note that the signal for three-lipid bound GIRK2 overlaps with the TPNQ-bound GIRK2, and four-lipid bound GIRK2 overlaps with the TPNQ-bound GIRK2 with one lipid also bound. (B) Ion mobility spectrum of the same species. The 17^{+} charge state species with TPNQ bound clearly demonstrates stabilized gas-phase arrival times. Resolution of all combinations is possible with mass spectrometry instruments with higher resolution.

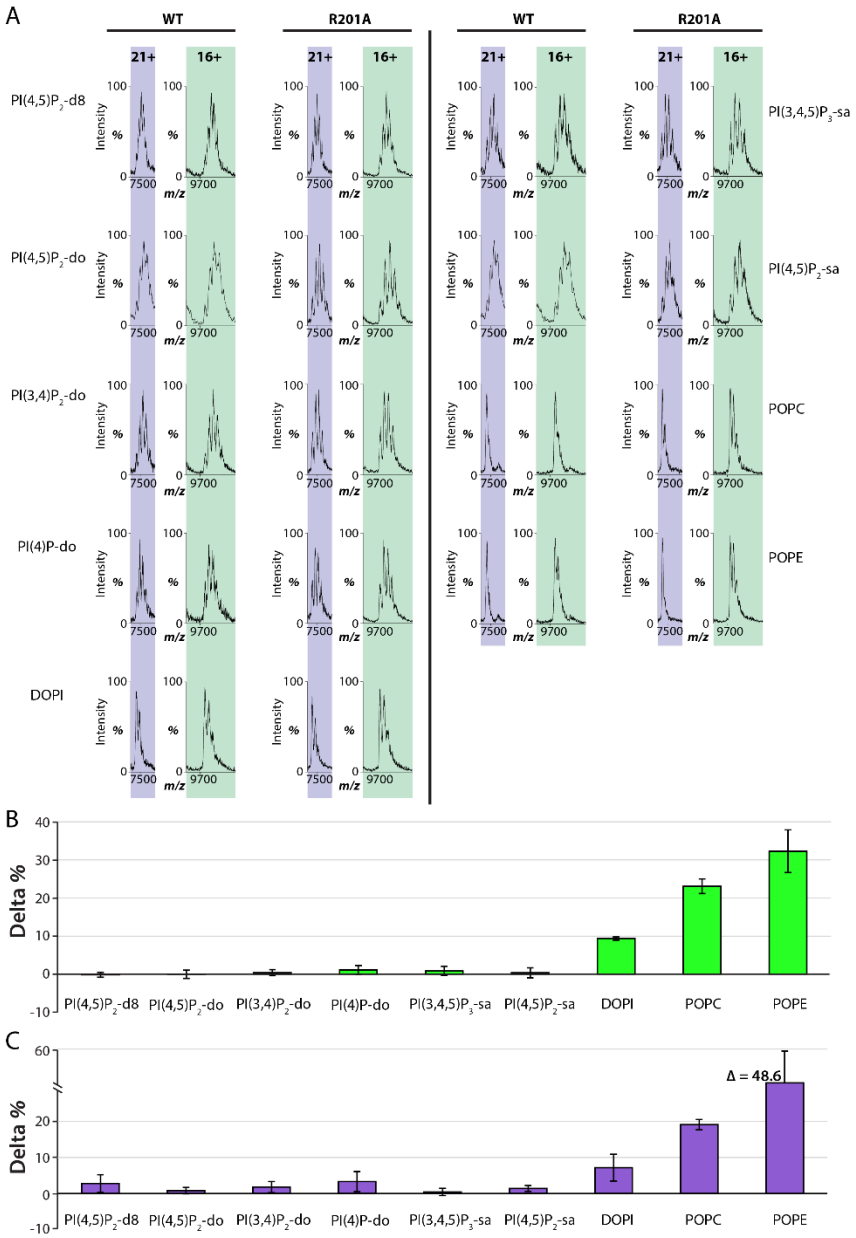

Figure 24. Comparison between partially activating (21^+) and native-like (16^+) charge states for different lipids bound to GIRK2. (A) Enlargement of regions of mass spectra for 21^+ and 16^+ charge states of GIRK2 and GIRK2^{R201A} bound to different lipids. For all PIPs, the fractional abundances of apo and lipid-bound GIRK2 are very similar between the two charge states. However, the other lipids (PI, PC and PE) display a dramatic reduction in the amount of lipid retained at the higher charge state. Calculated differences between the mole fraction of lipids bound to the 16^+ compared to the 21^+ charge state of (B) wild-type and (C) R201A mutant GIRK2.

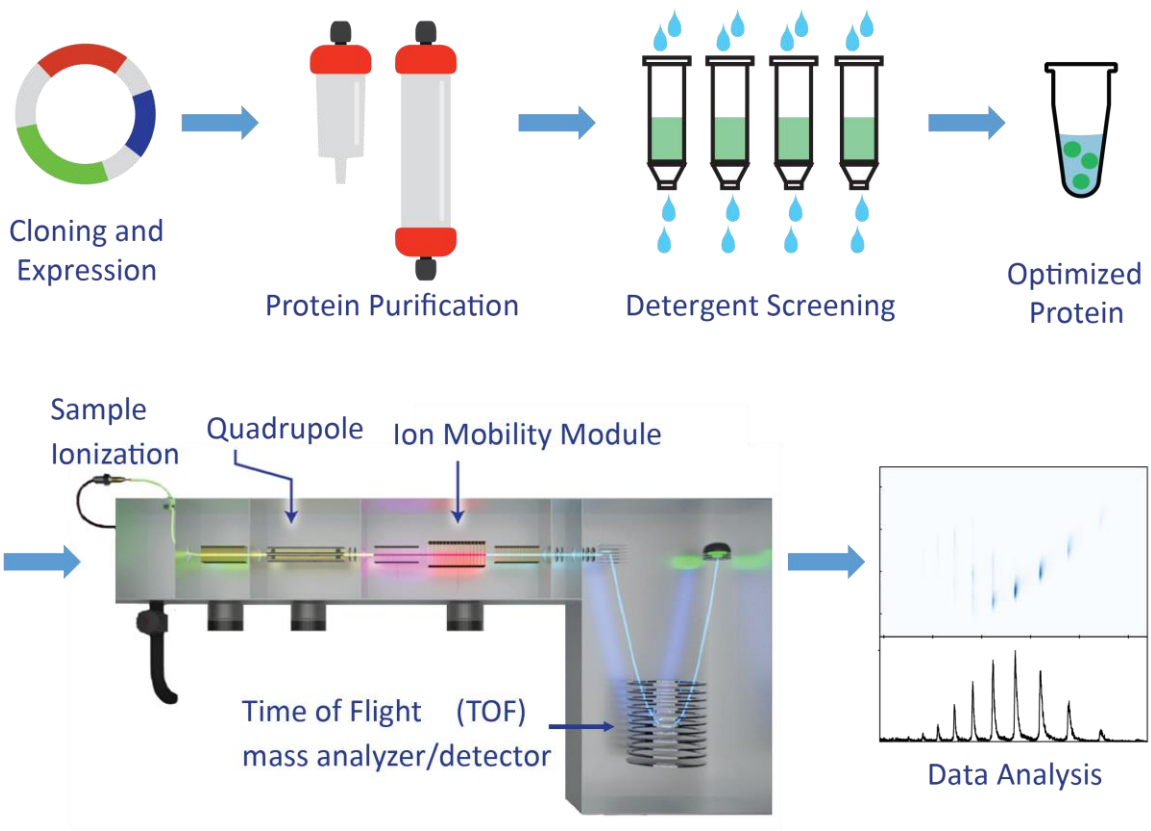

Figure 25. A generalized overview of the workflow of GIRK2 optimization for native MS studies. We performed screening of expression constructs, growth conditions, lysate treatment, purification conditions, detergent screens all as a part of the effort in obtaining better quality sample suitable for native mass spectrometry. The end goal is the unambiguous resolution of individual small molecules – all under 1,000 Da – bound to the intact 156,000 Da channel.

APPENDIX B

Table 1. Calculated and measured masses for GIRK2^{R201A} and GIRK2 bound to different ligands acquired on a Synapt G1 instrument. Measured mass was determined by deconvolution of native mass spectra using the program, UniDec.[95] For ligands bound to GIRK2, the addition of mass to the apo GIRK2 mass is reported. The reported standard deviation was calculated directly from the width of the zero-charge mass spectrum from UniDec after deconvolution.

Species	**Calculated Mass (Da)**	**Measured Mass (Da)**
GIRK2	156,292	156,296 ± 230
GIRK2 bound to:		
Tertiapin Q	Δ2,452	Δ2,450 ± 231
Ivermectin	Δ875	–
PI(4,5)P_2-d8	Δ798	Δ740 ± 320
PI(4,5)P_2-do	Δ1,074	Δ1,080 ± 351
PI(3,4)P_2-do	Δ1,074	Δ1,060 ± 353
PI(4)P_2-do	Δ977	Δ922 ± 372
DOPI	Δ880	Δ920 ± 361
PI(3,4,5)P_3-sa	Δ1,195	Δ1,060 ± 379
PI(4,5)P_2-sa	Δ1,098	Δ1,020 ± 375
POPC	Δ760	Δ802 ± 281
POPE	Δ718	Δ701 ± 357
GIRK2^{R201A}	155,952	155,989 ± 193

Table 2. Full name and abbreviations for lipids used in this study.

Lipid	Abbreviation	Acyl Chains
1,2-dioctanoyl-phosphatidylinositol-4',5'-bisphosphate	PI(4,5)P_2-d8	08:0-08:0
1,2-dioleoyl-phosphatidylinositol-4',5'-bisphosphate	PI(4,5)P_2-do	18:1-18:1
1,2-dioleoyl-phosphatidylinositol-3',4'-bisphosphate	PI(3,4)P_2-do	18:1-18:1
1,2-dioleoyl-phosphatidylinositol-4'-phosphate	PI(4)P_2-do	18:1-18:1
1,2-dioleoyl-phosphatidylinositol	DOPI	18:1-18:1
1-stearoyl-2-arachidonoyl- phosphatidylinositol-3',4',5'-bisphosphate	PI(3,4,5)P_3-sa	18:0-20:4
1-stearoyl-2-arachidonoyl- phosphatidylinositol-4',5'-bisphosphate	PI(4,5)P_2-sa	18:0-20:4
1-palmitoyl-2-oleoyl-phosphatidylcholine	POPC	16:0-18:1
1-palmitoyl-2-oleoyl-phosphatidylethanolamine	POPE	16:0-18:1